IEEE Access
Multidisciplinary | Rapid Review | Open Access Journal

Received December 20, 2019, accepted January 15, 2020, date of publication January 20, 2020, date of current version February 6, 2020.

Digital Object Identifier 10.1109/ACCESS.2020.2967873

Multistage Cooperative Trajectory Planning for Multimissile Formation via Bi-Level Sequential Convex Programming

CHAOYUE LIU, CHENG ZHANG, AND FENFEN XIONG

Key Laboratory of Dynamics and Control of Flight Vehicle, Ministry of Education, Beijing Institute of Technology, Beijing 100081, China

Corresponding author: Cheng Zhang (zhangcheng@bit.edu.cn)

This work was supported in part by the National Natural Science Foundation of China under Grant 11532002.

ABSTRACT Owing to the highly nonlinear dynamics and high number of nonlinear constraints, it is exceedingly difficult and computationally expensive to solve the cooperative trajectory planning problem of multimissile formation using existing approaches. To address this issue and improve the convergence property and computational efficiency, a bi-level sequential convex programming (SCP) method consisting of a system coordination level and an individual optimization level is proposed to solve the cooperative trajectory planning of missile formation. At the system level, the time consensus constraints are determined, the cooperative constraints that should be considered in the next iteration of the individual trajectory optimization level are identified, and the members that have converged are removed from the optimization sequence. As the number of members in the optimization sequence and the number of cooperative constraints considered in the individual SCP are clearly decreased, the convergence property and the computational efficiency of cooperative trajectory planning are evidently improved. At the individual level, the proposed method creatively proposes the innovative idea: based on the updated information of the system level, each member solves its individual trajectory optimization sub-problem independently and sequentially by gradually adding and tightening the cooperative constraints with the evolution of optimization iteration of SCP, which can further enhance the convergence property. Numerical simulations show that the proposed bi-level SCP method can effectively solve the multistage cooperative trajectory planning of multimissile formation with good convergence property, exhibiting the excellent scalability to the number of members and higher effectiveness. The comparison with the generation optimal control software (GPOPS) method further demonstrates the high efficiency of the proposed method.

INDEX TERMS Bi-level sequential convex programming, complex constraints, multistage cooperative trajectory planning, multimissile formation, time consensus.

I. INTRODUCTION

The cooperative attack of a missile formation presents better performance than that of an individual missile in penetrating defense systems, detecting maneuvering targets, and surviving the threats [1]–[4], and the cooperative attack has become an attractive and active research topic. As a key component of a cooperative attack, cooperative trajectory planning has gained significant attention. Typical cooperative trajectory planning methods include mixed-integer programming [5], nonlinear programming [6], rapidly exploring random tree [7], and heuristic-based intelligent methods [8]. However, as it is required to solve the trajectory optimization simultaneously for multiple flight vehicles during cooperative trajectory planning, these methods suffer from intensive computational cost, particularly when the number of flight vehicles is high.

Recently, the convex optimization has been widely employed in trajectory planning owing to its high efficiency in planetary powered soft landing [9]–[11], rendezvous and proximity operations [12], spacecraft coordination [13], control of swarms of spacecraft [14], formation reconfiguration [15], and entry trajectory optimization [16]. As most practical trajectory planning problems are highly nonlinear, it is

The associate editor coordinating the review of this manuscript and approving it for publication was Emanuele Crisostomi.

impossible to transform them to strictly convex optimization problems. In general, they cannot be solved in only one iteration using the convex optimization. Therefore, the sequential convex programming (SCP) approach has been developed through iteratively solving a series of convex programming sub-problems, which has demonstrated effectiveness in many practical optimal control problems. Regarding cooperative trajectory planning, several applications of SCP can be found in the literature. Based on SCP, Morgan *et al.* developed one centralized and two decentralized cooperative trajectory planning approaches for swarm reconfiguration of spacecraft with nonlinear dynamics [17]. Further, within the decentralized framework proposed in [17], the model predictive control (MPC) theory was integrated with SCP to reduce the computational cost and increase the anti-interference capability of the reconfiguration of a variable swarm [18]. Moreover, Augugliaro *et al.* applied SCP to an unmanned aerial vehicle (UAV) formation to solve cooperative trajectory planning considering the collision-avoidance constraint [19]. To achieve better computational tractability, Chen *et al.* developed a decoupled cooperative trajectory planning method based on SCP to sequentially generate the trajectory of each UAV [20].

In the aforementioned works on cooperative trajectory planning using SCP, the flight time of flight vehicles was assumed to be pre-specified. However, for a missile formation attacking a target, it is impossible to pre-specify the flight time of the missiles in practice. Very few studies on cooperative trajectory planning with free flight time exist in the literature. Meanwhile, in the cooperative attack scenario, multiple missiles are required to attack the target simultaneously to utilize formation advantage with the purpose of striking the enemy defense system and the target [21], [22]. To address this issue and to ensure the flight time consensus, Wang *et al.* proposed a decoupled cooperative trajectory planning approach for UAV formation, in which the decoupled sub-problems of trajectory optimization considering the constraint on time consensus for each member was solved with SCP [23]. However, the optimization sequence always contained all members during the optimization process, thus the computational cost increased significantly with the increase of the number of UAVs. Moreover, compared with a UAV or an agent, the velocity and flight space of a missile are significantly greater, and it is impossible for a missile to realize hovering and circling in the same manner as a UAV or an agent. In addition, the dynamics of a missile is more nonlinear and complicated. Therefore, the feasible region of optimization for the missile is significantly smaller and it is more sensitive to the initial values during optimization. So it is difficult to achieve SCP convergence, particularly when the number of missiles is large. These characteristics clearly increase the difficulty in solving the multi-constrained trajectory planning problem for missile formation via convex optimization.

Highly constrained trajectory optimization problems are usually difficult to solve. Chai *et al.* proposed a specific multiple-shooting discretization technique with the newest NSGA-III optimization algorithm and constructs a new evolutionary optimal control solver to solve the multiobjective trajectory planning problem with constraints and obtained the feasible trajectories [24]. Chai *et al.* employed a discretization technique to explore the optimal trajectories for a spacecraft entry flight planning scenario with probabilistic constraints and produced reliable and less conservative solutions [25].

On the other hand, during the missile formation flight, the corresponding cooperative trajectory planning problem is more complicated. It is required that the information of interception system be detected, the time of maneuvering penetration be determined, and the corresponding operational instructions for cooperative attack be generated, which indicates that the missiles should have formation-aggregation and formation-maintenance abilities. Therefore, the cooperative attack process of a missile formation has multiple stages, including formation aggregation, formation maintenance, formation penetration, and cooperative attack. For the multistage missile formation, different performance indices and constraints should be considered at different stages; evidently, this increases the complexity and difficulty of cooperative trajectory planning.

In this work, to address the aforementioned issues and improve the convergence property and computational efficiency, a bi-level SCP (Bil-SCP) method comprising both the system and the individual level, is developed to solve the cooperative trajectory optimization problem of missile formation considering multiple stages (i.e., formation aggregation, formation maintenance, formation penetration and cooperative attack). At the system level, missile members that have not achieved the time-consensus and states-convergence criteria are identified and retained in the optimization sequence. Meanwhile, the cooperative constraints of each member that have not been satisfied in the previous iteration are also identified. In addition, the constraints on the flight time consensus are determined for each member. Then, the trajectory optimization sub-problem is solved for each member in the optimization sequence at its individual level independently and sequentially, considering the identified cooperative constraints at the system level and the previously determined flight time-consensus constraint. Once one missile member has completed its optimization, it will broadcast its current optimal trajectory to the remaining missile members in the optimization sequence; based on this optimal trajectory, the trajectory optimization of the remaining missiles could be carried out in turn, which is conducive to the convergence to a better solution.

As the number of missiles participating in the optimization gradually decreased with the evolution of iterations and the decrease in the number of constraints, the computational efficiency and the convergence property noticeably improve in the cooperative trajectory optimization with the proposed Bil-SCP method, which was beneficial to the expansion of

formation size. To further improve the convergence property of SCP, at the individual level, the Bil-SCP method creatively proposes the innovative idea: the convex cooperative constraints are gradually tightened up and included into the optimization with the evolution of the optimization iteration of the SCP, and thus to form a sequence of more relaxed and feasible intermediate optimization problems to avoid the over-constrained optimization problem caused by simultaneously introducing a large number of conservative convex cooperative constraints. Furthermore, to guarantee the free flight time of each stage for the members, the flight time is set as a separate decision variable in the SCP optimization.

The remainder of this article is organized as follows. In Section 2, the initial non-convex multistage cooperative trajectory planning problem with free flight time for multimissile formation will be established. In Section 3, the convexification techniques that transform the original trajectory planning problem to a convex one will be described. The proposed bi-level cooperative trajectory planning method based on the SCP theory, including the system coordination level and the individual level, will be presented in Section 4. In Section 5, the numerical simulation results will be presented to illustrate the effectiveness of the proposed Bil-SCP method. Finally, the conclusions will be presented in Section 6.

II. PROBLEM DESCRIPTION

In this section, the optimal control model of multistage cooperative trajectory planning with free flight time for multimissile formation will be established. In this work, the process of the missile-formation cooperative attack is divided into four successive stages: formation aggregation, formation maintenance, formation penetration and cooperative attack. For formation aggregation, all missile members fly to a specified region, in which collision avoidance and no-fly zone avoidance must be considered. Formation maintenance refers to the process that all members fly in a fixed formation within the allowable error range until certain members detect the interceptor missiles. Formation penetration is the process during which members maneuver to escape the interceptor missiles. Cooperative attack refers to the process of simultaneous cooperative attack on the assigned target, according to the specified terminal requirements. Meanwhile, the flight time of each stage is not limited to a specific duration.

A. MISSILE DYNAMICS

At each flight stage, the dynamics of each formation member is the same, as shown in Eq.(1). The fixed coordinate system is established, in which the x-axis and y-axis point to the east and vertically upward, respectively; the z-axis is such that the coordinate system satisfies the right-hand rule. For a multimissile formation with N_m members, the dimensionless dynamics for each member is as the following.

$$\begin{cases} \dot{V} = -D - \sin\theta/r^2 \\ \dot{\theta} = L\cos\sigma/V - \cos\theta/Vr^2 \\ \dot{\psi} = -L\sin\sigma/(V\cos\theta) \\ \dot{x} = V\cos\theta\cos\psi \\ \dot{y} = V\sin\theta \\ \dot{z} = -V\cos\theta\sin\psi, \end{cases} \tag{1}$$

where (x, y, z) denotes the position coordinate of the missile scaled by the radius of the earth R_0, $r = 1 + y$ represents the radial distance from the earth center to the missile, V denotes the velocity scaled by $\sqrt{g_0 R_0}$ (g_0 is the earth gravitational acceleration at R_0), the heading angle ψ is measured clockwise from the east, θ is the flight path angle, and σ is the bank angle.

The differentiation is with respect to the dimensionless time, t, scaled by $\sqrt{R_0/g_0}$. The dimensionless lift acceleration, L, and the dimensionless drag acceleration, D, are

$$\begin{aligned} L &= 0.5R_0\rho V^2 S_{ref} C_L(\alpha, Ma)/m_{ref} \\ D &= 0.5R_0\rho V^2 S_{ref} C_D(\alpha, Ma)/m_{ref}, \end{aligned} \tag{2}$$

where ρ is the atmospheric density, S_{ref} is the reference area, m_{ref} is the reference mass, C_D and C_L are the drag and lift coefficients, respectively.

It is apparent that the dynamics equations shown in Eq. (1)are nonlinear; hence, they need convexification for the application of the convex programming method. Therefore, the following drag polar is used:

$$C_D(\alpha, Ma) = C_{D0}(Ma) + Km(Ma)\cdot[C_L(\alpha, Ma)]^2, \tag{3}$$

where the zero-lift drag coefficient, C_{D0}, and the induced drag factor, Km, can be determined by interpolating the aerodynamic coefficients.

Based on Eq. (3), the lift and drag coefficients corresponding to the maximum lift-to-drag ratio can be obtained as follows.

$$\begin{aligned} \hat{C}_L(Ma) &= \sqrt{C_{D0}(Ma)/Km(Ma)} \\ \hat{C}_D(Ma) &= 2C_{D0}(Ma) \end{aligned} \tag{4}$$

A normalized lift coefficient is defined:

$$\eta = C_L(\alpha, Ma)/\hat{C}_L(Ma). \tag{5}$$

Substituting Eq. (5)into Eq. (4) yields

$$C_D(\alpha, Ma) = 0.5\hat{C}_D(Ma)[1 + \eta(\alpha, Ma)^2]. \tag{6}$$

By combining Eq. (5) and Eq(6)., both C_L and C_D are functions of η. Correspondingly, L and D are functions of η as well.

$$\begin{aligned} L &= \hat{L}(Ma)\eta(\alpha, Ma) \\ D &= 0.5\hat{D}(Ma)[1 + \eta(\alpha, Ma)^2], \end{aligned} \tag{7}$$

where $\hat{L}$ and $\hat{D}$ are the dimensionless lift and drag accelerations corresponding to $\hat{C}_L$ and $\hat{C}_D$, respectively.

A new control vector, $\boldsymbol{u} = [u_1, u_2, u_3]^T$, is defined.

$$u_1 = \eta\cos\sigma, \quad u_2 = \eta\sin\sigma, \ u_3 = \eta^2 \tag{8}$$

Obviously, the control variables must satisfy the following condition:

$$u_1^2 + u_2^2 = u_3. \tag{9}$$

In addition, constraints must be applied on u_1, u_2 and u_3, as α and σ are constrained. In this work, it is assumed that the lift coefficient of the missile is non-negative, i.e., $\eta > 0$, and that the upper bound of η could be determined by the maximum allowable angle of attack:

$$0 \le \eta \le \tilde{\eta}(Ma), \tag{10}$$

where η is the upper bound.

Thus

$$0 \le u_3 \le \tilde{u}_3, \tag{11}$$

where $\tilde{u}_3 = [\tilde{\eta}(Ma)]^2$.

It is assumed that the bank angle, σ, is within $[-180, 180]$ deg. Thus, the control constraints can be expressed as

$$\boldsymbol{u} \in \{u_1^2 + u_2^2 = u_3, 0 \le u_3 \le \tilde{u}_3\}. \tag{12}$$

After $\boldsymbol{u}$ is obtained, the initial control variables α and σ can be inversely deduced. To obtain α, η is first computed:

$$\eta = \sqrt{u_3}. \tag{13}$$

Using Eq.(5), $C_L(\alpha, Ma)$ can be calculated. When Ma is determined, the corresponding α can be found through the obtained $C_L(\alpha, Ma)$. To obtain σ, $\cos\sigma$ and $\sin\sigma$ are first computed as follows:

$$\cos\sigma = \frac{u_1}{\eta}, \quad \sin\sigma = \frac{u_2}{\eta}. \tag{14}$$

Then, the value of σ can be calculated. It should be noted that typically $\eta \neq 0$, otherwise $u_1 = u_2 = u_3 = 0$.

For simplicity, the states and controls of the i^{th} member in the missile formation are defined as $\boldsymbol{x}_i = [V_i, \theta_i, \psi_i, x_i, y_i, z_i]^T$ and $\boldsymbol{u}_i = [u_{1i}, u_{2i}, u_{3i}]^T$ $(i = 1, 2, \ldots, N_m$, N_m is the number of formation members), respectively. Then, the aforementioned nonlinear dynamics (Eq. (1)) and control constraints can be expressed as

$$\dot{\boldsymbol{x}}_i = \boldsymbol{f}(\boldsymbol{x}_i, \boldsymbol{u}_i), \tag{15}$$

$$\boldsymbol{u}_i \in \{u_{1i}^2 + u_{2i}^2 = u_{3i}, 0 \le u_{3i} \le \tilde{u}_{3i}\}. \tag{16}$$

The formation is intercepted by interceptor missiles during flight. In this work, it is assumed that the interceptor missile employs proportional guidance as commonly practiced, and its dynamics equations are

$$\begin{cases} \dot{V}_I = a_{xI} \\ \dot{\theta}_I = a_{yI}/V_I \\ \dot{\psi}_I = a_{zI}/(V_I\cos\theta_I) \\ \dot{x}_I = V_I\cos\theta_I\cos\psi_I \\ \dot{y}_I = V_I\sin\theta_I \\ \dot{z}_I = -V_I\cos\theta_I\sin\psi_I, \end{cases} \tag{17}$$

where a_{xI} is the axial acceleration of the interceptor missile that has been estimated via the formation cooperative detection; a_{yI} and a_{zI} are the accelerations along the y- axis and z–axis, respectively, and are determined by proportional navigation.

The state vector of the n^{th} interceptor missile is denoted as $\boldsymbol{x}_{I,n} = [V_{I,n}, \theta_{I,n}, \psi_{I,n}, x_{I,n}, y_{I,n}, z_{I,n}]^T$ $(n = 1, 2...N_I)$, where N_I is the number of the interceptor missiles.

B. CONSTRAINTS

1) PATH CONSTRAINTS

To ensure safety, the dynamic pressure and normal overload of missile members are constrained as the following:

$$\begin{cases} q_i = 0.5 g_0 R_0 \rho_i V_i^2 \le q_{\max} \\ n_{L,i} = 0.5 R_0 \rho_i V_i^2 S_{ref} C_L \big/ m_{ref} \le n_{L\max} \\ i = 1, 2, \ldots, N_m. \end{cases} \tag{18}$$

The exponential atmospheric density model is used [26], as shown below.

$$\rho_i = \rho_0 e^{-\beta R_0 y_i}, \tag{19}$$

where $\rho_0 = 1.225$ and $\beta = 1/7201$.

The Eq. (18) can be rewritten as

$$\begin{cases} V_i \le \tilde{V}_{q,i} \\ V_i \le \tilde{V}_{nL,i}, \end{cases} \tag{20}$$

where $\tilde{V}_{q,i} = \sqrt{2q_{\max}/\rho_i}\Big/\sqrt{g_0 R_0}$ and $\tilde{V}_{nL,i} = \sqrt{2n_{L\max} m_{ref}/\rho_i S_{ref} R_0 C_L}$.

2) COOPERATIVE CONSTRAINTS

Collision avoidance constraints: it is required that the distance between any two missile members is always greater than the safe distance, R_s:

$$\left\| \boldsymbol{C}_1 \cdot [\boldsymbol{x}_i(t) - \boldsymbol{x}_j(t)] \right\| \ge R_s, \quad i, j = 1, 2, \ldots, N_m, \ i \neq j, \tag{21}$$

where matrix $\boldsymbol{C}_1 = diag(0, 0, 0, 1, 1, 1)$ is used to extract the space position of the missiles and $\|\cdot\|$ represents the distance between any two missiles.

No-fly zone avoidance constraints: to improve the survivability, the members should always be located outside all no-fly zones. In the present research work, the cylinder model with an infinite height is used to represent the no-fly zone.

$$\left\| \boldsymbol{C}_2 \cdot \boldsymbol{x}_i(t) - \boldsymbol{p}_{nfz,l} \right\| \ge R_{n,l}, \quad i = 1, 2, \ldots, N_m, \quad l = 1, 2, \ldots, N_n, \tag{22}$$

where matrix $\boldsymbol{C}_2 = diag(0, 0, 0, 1, 1, 0)$ is used to extract the horizontal position of the members, N_n is the number of the no-fly zones, and $\boldsymbol{p}_{nfz,l}$ and $R_{n,l}$ are the horizontal position and the radius of the l^{th} no-fly zone, respectively.

Interceptor missile avoidance constraints: at the penetration stage, to achieve maneuvering penetration, each member

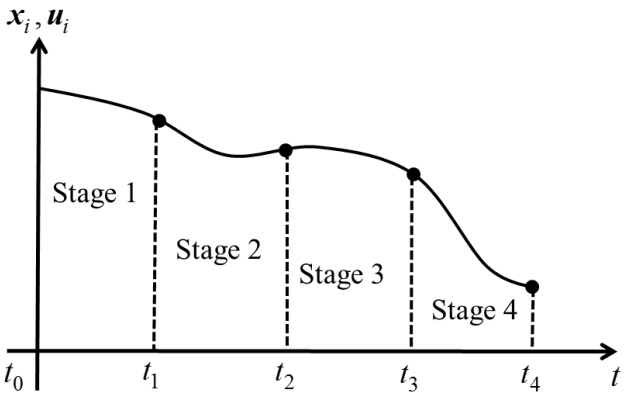

FIGURE 1. Continuity of stages.

should always be outside the damage range, R_I, of the interceptor missiles.

$$\left\|\boldsymbol{C}_1 \cdot [\boldsymbol{x}_i(t) - \boldsymbol{x}_{I,n}(t)]\right\| \geq R_I, \quad i = 1, 2, \ldots, N_m, \quad n = 1, 2, \ldots, N_I, \tag{23}$$

where the positions of the interceptor missiles are predicted via the formation cooperative detection.

3) BOUNDARY CONSTRAINTS

The boundary constraints for each flight stage for formation members are determined according to the mission, which, are expressed as follows in general.

$$\Phi_{\min,i,p} \leq \Phi(\boldsymbol{x}_i(t_{p-1}), t_{p-1}, \boldsymbol{x}_i(t_p), t_p) \leq \Phi_{\max,i,p}, \tag{24}$$

where $p = 1, 2, 3, 4$ is the number of flight stages, t_0 is the initial time, and t_1, t_2, t_3, and t_4 are the terminal times of the first to the fourth stage, respectively.

4) MULTISTAGE CONNECTION CONSTRAINTS

In multistage trajectory planning, it is necessary to ensure the close connection of the time and the states between adjacent stages, as shown in Fig. 1. Therefore, mandatory connection constraints need to be applied to the stage boundary.

$$M(\boldsymbol{x}_i(t_p), \boldsymbol{u}_i(t_p), t_p) = \begin{bmatrix} \boldsymbol{x}_i(t_p^-) - \boldsymbol{x}_i(t_p^+) \\ \boldsymbol{u}_i(t_p^-) - \boldsymbol{u}_i(t_p^+) \end{bmatrix} = 0, \tag{25}$$

where $p = 1, 2, 3$ is the number of stages.

C. OPTIMAL CONTROL MODEL

The performance index of the first three stages is the minimum energy consumption, and the performance index of the last stage is the maximum terminal velocity to achieve the greatest damage effect on the targets. Then, the initial optimal control problem, $\mathbf{P}_1$, for the cooperative trajectory optimization of the missile formation is formulated as in the following.

$$\min_{i=1,2,\ldots N_m} \begin{cases} \sum_{i=1}^{N_m} \int_{t_{p-1}}^{t_p} u_{3i} \mathrm{d}t, & p = 1, 2, 3 \\ -V_i(t_4), & p = 4 \end{cases}$$

$$\text{s.t.:} \begin{cases} (15)(16)(20) \sim (22)(24)(25), & p = 1, 2; \\ (15)(16)(20) \sim (25), & p = 3; \\ (15)(16)(20)(22)(24)(25), & p = 4. \end{cases} \tag{26}$$

where the difference $t_{p-1} - t_p (p = 1, 2, 3, 4)$ denotes the flight time of the p^{th} stage, which is set as a separate decision variable in the optimization to guarantee that the flight time of each stage is free.

III. CONVEXIFICATION

The SCP technique is an iterative method to solve a series of convex programming problems [14]. When SCP is used to solve optimal control problems, a guessed initial nominal state should be provided in the first iteration. In each iteration, convex programming is employed to solve the optimal control problem, of which the obtained optimal solution is considered as the nominal guess for the convex programming in the following iteration. The SCP iterations continue until the states converge. To apply SCP to solve the aforementioned cooperative trajectory planning problem, convexifation techniques should be employed in the optimal control problem, $\mathbf{P}_1$, to establish a convex trajectory planning problem. Linearization and discretization should be performed on the missile dynamics to achieve convexification, and convexification should also be performed on the cooperative constraints. Furthermore, convex relaxation is used for the equivalent reconstruction of the convex trajectory planning problem.

A. LINEARIZATION AND DISCRETIZATION OF DYNAMICS

Because the dynamic equations of each stage are identical in form, the subscript p, which denotes the flight stage, is omitted when introducing linearization and discretization.

1) LINEARIZATION

It is assumed that the optimal solution obtained in the m^{th} optimization iteration of SCP is $\{\boldsymbol{x}_i^m; \boldsymbol{u}_i^m\}$, around which the nonlinear dynamics shown in Eq. (15) employed in the $(m+1)^{\text{th}}$ iteration is approximated as a linear one:

$$\dot{\boldsymbol{x}}_i = \boldsymbol{A}_i^m(\boldsymbol{x}_i^m, \boldsymbol{u}_i^m)\boldsymbol{x}_i + \boldsymbol{B}_i^m(\boldsymbol{x}_i^m, \boldsymbol{u}_i^m)\boldsymbol{u}_i + \boldsymbol{c}_i^m(\boldsymbol{x}_i^m, \boldsymbol{u}_i^m), \tag{27}$$

where $\boldsymbol{A}_i^m(\boldsymbol{x}_i^m, \boldsymbol{u}_i^m) = \partial \boldsymbol{f}(\boldsymbol{x}_i, \boldsymbol{u}_i)/\partial \boldsymbol{x}_i \Big|_{\{\boldsymbol{x}_i^m;\, \boldsymbol{u}_i^m\}}$ and $\boldsymbol{B}_i^m(\boldsymbol{x}_i^m, \boldsymbol{u}_i^m) = \partial \boldsymbol{f}(\boldsymbol{x}_i, \boldsymbol{u}_i)/\partial \boldsymbol{u}_i \Big|_{\{\boldsymbol{x}_i^m;\, \boldsymbol{u}_i^m\}}$.

To ensure the accuracy of the aforementioned linearization, a confidence region is required to be considered.

$$\left|\boldsymbol{x}_i - \boldsymbol{x}_i^m\right| \leq \boldsymbol{\varepsilon}, \quad \boldsymbol{\varepsilon} \in \boldsymbol{R}^6, \tag{28}$$

where $\boldsymbol{\varepsilon}$ is a constant vector.

2) DISCRETIZATION

The flight time of each stage, $t_p - t_{p-1}$ $(p = 1, 2, 3, 4)$, is set as a decision variable to guarantee the free final time of each stage, which is divided into K intervals with a time step of $\Delta t = (t_p - t_{p-1})/K, (p = 1, 2, 3, 4)$. Then, each stage of the

trajectory is discretized into $K+1$ points in the time interval $[t_{p-1}, t_p]$, and $t_k = t_{p-1} + k \cdot \Delta t$ $(k = 0, 1, 2, \ldots, K)$. States and controls are discretized as $\boldsymbol{x}_i[k] = \boldsymbol{x}_i(t_k)$ and $\boldsymbol{u}_i[k] = \boldsymbol{u}_i(t_k)$, respectively. Based on the trapezoidal numerical integration method, the linearized dynamic equations shown in Eq. (27) are further discretized.

$$\begin{aligned}&\boldsymbol{G}^m_{i,k+1} \cdot \boldsymbol{x}_i[k+1] + \boldsymbol{G}^m_{i,k} \cdot \boldsymbol{x}_i[k] \\ &\quad + \boldsymbol{H}^m_{i,k+1} \cdot \boldsymbol{u}_i[k+1] + \boldsymbol{H}^m_{i,k} \cdot \boldsymbol{u}_i[k] \\ &\quad + (\boldsymbol{E}^m_{i,k} + \boldsymbol{E}^m_{i,k+1}) \cdot \Delta t + \boldsymbol{F}^m_{i,k} + \boldsymbol{F}^m_{i,k+1} = 0, \\ &\quad k = 0, 1, \ldots K,\end{aligned} \tag{29}$$

where

$$\begin{aligned}\boldsymbol{G}^m_{i,k} &= 0.5\Delta\bar{t} \cdot \boldsymbol{A}^m_{i,k} + \boldsymbol{I}, \\ \boldsymbol{G}^m_{i,k+1} &= 0.5\Delta\bar{t} \cdot \boldsymbol{A}^m_{i,k+1} + \boldsymbol{I}, \\ \boldsymbol{H}^m_{i,k} &= 0.5\Delta\bar{t} \cdot \boldsymbol{B}^m_{i,k} \\ \boldsymbol{H}^m_{i,k+1} &= 0.5\Delta\bar{t} \cdot \boldsymbol{B}^m_{i,k+1}, \\ \boldsymbol{E}^m_{i,k} &= 0.5\boldsymbol{f}(\boldsymbol{x}^m_i[k], \boldsymbol{u}^m_i[k]), \\ \boldsymbol{E}^m_{i,k+1} &= 0.5\boldsymbol{f}(\boldsymbol{x}^m_i[k+1], \boldsymbol{u}^m_i[k+1]), \\ \boldsymbol{F}^m_{i,k} &= -0.5\Delta\bar{t} \cdot \left(\boldsymbol{A}_k \cdot \boldsymbol{x}^m_i[k] + \boldsymbol{B}_k \cdot \boldsymbol{u}^m_i[k]\right), \\ \boldsymbol{F}^m_{i,k+1} &= -0.5\Delta\bar{t} \\ &\quad \cdot \left(\boldsymbol{A}_{k+1} \cdot \boldsymbol{x}^m_i[k+1] + \boldsymbol{B}_{k+1} \cdot \boldsymbol{u}^m_i[k+1]\right),\end{aligned} \tag{30}$$

$\boldsymbol{A}^m_{i,k}$ and $\boldsymbol{B}^m_{i,k}$ are the values of Jacobian matrices $\boldsymbol{A}^m_i(\boldsymbol{x}^m_i, \boldsymbol{u}^m_i)$ and $\boldsymbol{B}^m_i(\boldsymbol{x}^m_i, \boldsymbol{u}^m_i)$ at the k^{th} discrete point, respectively.

B. CONVEXIFICATION OF COOPERATIVE CONSTRAINTS

As the current collision avoidance constraints shown in Eq. (21) are non-convex, it is necessary to convert them into convex ones. The following inequalities offer sufficient conditions for the collision avoidance constraints among all formation members [17].

$$\begin{aligned}&(\bar{\boldsymbol{x}}_i[k] - \bar{\boldsymbol{x}}_j[k])^T \cdot \boldsymbol{C}_1^T \boldsymbol{C}_1 \cdot (\boldsymbol{x}_i[k] - \boldsymbol{x}_j[k])^T \\ &\quad \geq R_s \cdot \left\|\boldsymbol{C}_1 \cdot \bar{\boldsymbol{x}}_i[k] - \boldsymbol{C}_1 \cdot \bar{\boldsymbol{x}}_j[k]\right\| \\ &\quad i, j = 1, 2, \ldots, N_m, \quad i \neq j, \ k = 1, 2, \ldots, K\end{aligned} \tag{31}$$

The original cylinder no-fly zone avoidance constraints (Eq. (22)) can be convexified into half-plane affine constraints [17] at all discrete points of the nominal trajectory, as in below.

$$\begin{aligned}&\left\|\boldsymbol{C}_2 \cdot \bar{\boldsymbol{x}}_i[k] - \boldsymbol{p}_{nfz,l}\right\| \\ &\quad + \frac{(\boldsymbol{C}_2 \cdot \bar{\boldsymbol{x}}_i[k] - \boldsymbol{p}_{nfz,l})^T}{\left\|\boldsymbol{C}_2 \cdot \bar{\boldsymbol{x}}_i[k] - \boldsymbol{p}_{nfz,l}\right\|} \cdot (\boldsymbol{C}_2 \cdot \boldsymbol{x}_i[k] - \boldsymbol{C}_2 \cdot \bar{\boldsymbol{x}}_i[k]) \geq R_{n,l} \\ &\quad i = 1, 2, \ldots, N_m, \quad l = 1, 2, \ldots, N_n, \ k = 1, 2, \ldots, K\end{aligned} \tag{32}$$

However, it can be seen from Eq. (32) that the no-fly zone avoidance constraints only function at discrete points; hence, the trajectory between discrete points may not satisfy the constraints. Therefore, the following constraints are added to ensure that the trajectory between the discrete intervals also satisfies the constraints.

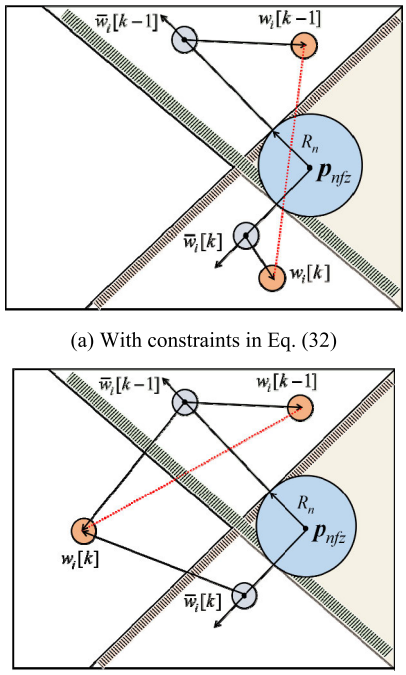

(a) With constraints in Eq. (32)

(b) With constraints in Eqs. (32) and (33)

FIGURE 2. Convexification of no-fly-zone avoidance constraints.

$$\begin{aligned}&\left\|\boldsymbol{C}_2 \cdot \bar{\boldsymbol{x}}_i[k-1] - \boldsymbol{p}_{nfz,l}\right\| \\ &\quad + \frac{(\boldsymbol{C}_2 \cdot \bar{\boldsymbol{x}}_i[k-1] - \boldsymbol{p}_{nfz,l})^T}{\left\|\boldsymbol{C}_2 \cdot \bar{\boldsymbol{x}}_i[k-1] - \boldsymbol{p}_{nfz,l}\right\|} \cdot (\boldsymbol{C}_2 \cdot \boldsymbol{x}_i[k] - \boldsymbol{C}_2 \cdot \bar{\boldsymbol{x}}_i[k-1]) \geq R_{n,l} \\ &\quad i = 1, 2, \ldots, N_m, \quad l = 1, 2, \ldots, N_n, \ k = 1, 2, \ldots, K\end{aligned} \tag{33}$$

Fig. 2 depicts the geometric description of the no-fly-zone avoidance constraints at the discrete points and between discrete points after convexification, where the larger blue circle denotes the no-fly zone and the left blank area denotes the feasible zone after convexification. As shown in Fig. 2, according to the constraints shown in Eq. (32), new positions, i.e., $w_i[k-1]$ and $w_i[k]$, are obtained by referring to the corresponding nominal positions $\bar{w}_i[k-1]$ and $\bar{w}_i[k]$ with respect to the $(k\text{-}1)^{\text{th}}$ and k^{th} discrete points, respectively. As shown in Fig. 2 (a), the trajectory between the two adjacent discrete points (i.e., $w_i[k-1]$ and $w_i[k]$)—denoted by the red dotted line—passes through the no-fly zone. However, as shown in Fig. 2 (b), if constraints shown in Eq. (33) are further considered, the line segments between the adjacent discrete points ($w_i[k-1]$ and $w_i[k]$) clearly no longer intersect with the interior of the no-fly zone, which ensures the security of trajectory.

At the penetration stage, to avoid interceptor missiles, it is necessary to ensure that the position of each member is outside the damage range, R_I, of all interceptor missiles at all discrete points. After convexification, the interceptor missile

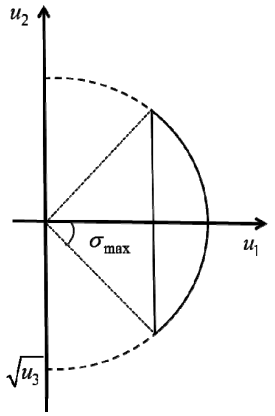

(a) Original non-convex set

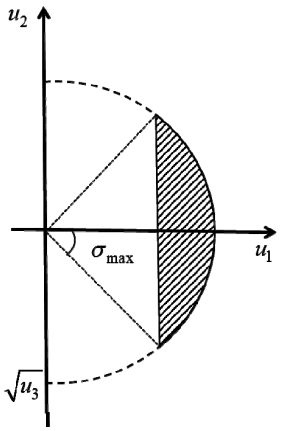

(b) Relaxed convex set

FIGURE 3. Relaxation of control constraints.

avoidance constraints at the discrete points are

$$\begin{aligned}&(\bar{\boldsymbol{x}}_i[k]-\boldsymbol{x}_{I,n}[k])^T\cdot\boldsymbol{C}_1^T\boldsymbol{C}_1\cdot(\boldsymbol{x}_i[k]-\boldsymbol{x}_{I,n}[k])^T\\&\quad\geq R_I\cdot\left\|\boldsymbol{C}_1\cdot\bar{\boldsymbol{x}}_i[k]-\boldsymbol{C}_1\cdot\boldsymbol{x}_{I,n}[k]\right\|\\&\qquad i=1,2,\ldots,N_m,\quad n=1,2,\ldots,N_I,\ k=1,2,\ldots,K.\end{aligned}\tag{34}$$

C. CONVEX RELAXATION OF CONSTRAINTS

From Eq.(16), it may be noticed that the control constraints in the optimal control problem, $\mathbf{P}_1$, are non-convex. Therefore, the equality constraints in Eq. (16) are transformed into convex inequality constraints, as shown below, using the convex relaxation technique, as illustrated in Fig. 3. It is obvious that the original non-convex set consists of one solid arc segment on the semicircle, and the relaxed convex set consists of the shaded area, including the boundaries.

$$\boldsymbol{u}_i\in\{u_{1i}^2+u_{2i}^2\leq u_{3i},0\leq u_{3i}\leq\tilde{u}_{3i}\}\tag{35}$$

D. FORMATION OF THE CONVEX PROGRAMMING PROBLEM

By employing the linearization, discretization, and convexification presented previously, a convex programming problem, $\mathbf{P}_2$, for the multistage cooperative trajectory optimization is formed, as shown below.

$$\begin{aligned}&\min_{i=1,2,\ldots N_m}\begin{cases}\sum_{i=1}^{N_m}\sum_{k=1}^{K}(u_{3i}\cdot\Delta t), & p=1,2,3\\ -V_i(t_4), & p=4\end{cases}\\&\text{s.t.:}\begin{cases}(20)(24)(25)(29)(31)\sim(33)(35), & p=1,2;\\ (20)(24)(25)(29)(31)\sim(35), & p=3;\\ (20)(24)(25)(29)(32)(33)(35), & p=4.\end{cases}\end{aligned}\tag{36}$$

E. ASSURANCE OF EXACT CONVEX RELATION

As may be noticed in Eq.(35), the relaxation of controls may not guarantee $(u_{1i}^*)^2+(u_{2i}^*)^2=u_{3i}^*$. Therefore, the scenario of the regularization term is introduced to problem $\mathbf{P}_2$, and a regularization term of the heading angle integral is added to the performance index for the last stage, which yields $\mathbf{P}_3$:

$$\begin{aligned}&\min_{i=1,2,\ldots N_m}\begin{cases}\sum_{i=1}^{N_m}\sum_{k=1}^{K}(u_{3i}\cdot\Delta t), & p=1,2,3\\ -V_i(t_4)+c_\psi\int_{t_3}^{t_4}\psi_i\mathrm{d}t, & p=4\end{cases}\\&\text{s.t.:}\begin{cases}(20)(24)(25)(29)(31)\sim(33)(35), & p=1,2;\\ (20)(24)(25)(29)(31)\sim(35), & p=3;\\ (20)(24)(25)(29)(32)(33)(35), & p=4.\end{cases}\end{aligned}\tag{37}$$

where c_ψ is selected to make $c_\psi\int_{t_3}^{t_4}\psi_i\mathrm{d}t$ sufficiently small, compared with the magnitude of $V_i(t_4)$.

Although the magnitude of the regularization term is very small, based on Lemma 1, the solution of problem $\mathbf{P}_3$ can guarantee the exactness of the convex relaxation.

Lemma 1: If $\{\boldsymbol{x}_i^*;\boldsymbol{u}_i^*\}$ is the optimal solution of problem $\mathbf{P}_3$, $(u_{1i}^*)^2(u_{2i}^*)^2=u_{3i}^*$ is always satisfied within $[t_0,t_4]$.

Proof of Lemma 1 can be found in Appendix.

In combination with **Lemma 1**, the only difference between $\mathbf{P}_2$ and $\mathbf{P}_3$ is the regularization term in the performance index; the magnitude of the regularization term can be sufficiently small by selecting a small c_ψ value. It can be derived that $\{\boldsymbol{x}_i^*;\boldsymbol{u}_i^*\}$ is a near-optimal solution of $\mathbf{P}_2$ with $(u_{1i}^*)^2+(u_{2i}^*)^2=u_{3i}^*$ satisfied; then, $\{\boldsymbol{x}_i^*;\boldsymbol{u}_i^*\}$ is also a near-optimal solution of $\mathbf{P}_1$.

IV. THE PROPOSED BI-LEVEL SCP METHOD

In this section, a cooperative trajectory planning method based on SCP (referred to as Bil-SCP) that consists of the system level and the individual level, is described in detail. The flow chart of the proposed method is shown in Fig. 4. To address the sensitivity issue to the initial values, the trajectory optimization sub-problem of each member without considering the time consensus and the cooperative constraints is solved first; and its optimal solution is passed to subsequent SCP as initial values.

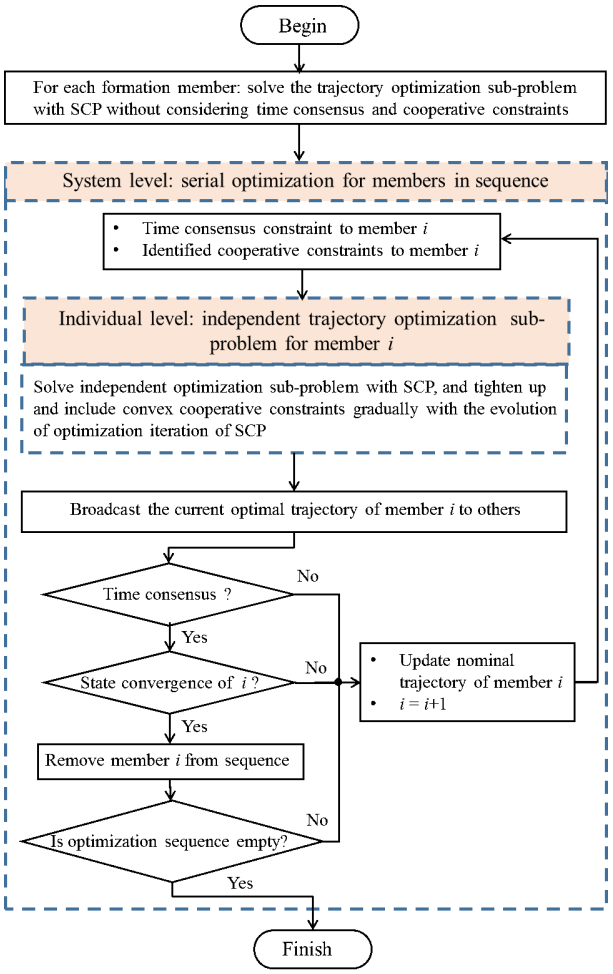

FIGURE 4. Flowchart of the proposed Bil-SCP method.

At system level, three tasks should be accomplished. First, the missile members that have achieved the time-consensus and states-convergence criteria are identified and removed from the optimization sequence. Second, the constraints on time consensus are determined and updated for each member in the optimization sequence (please refer to the inequality relation, Eq. (39)).

As the trajectory of each member is optimized independently, the time-step size of different members may be different. To ensure the flight time consensus, the following constraints must be met.

$$\max_{i=1,2,\ldots N_m} \Delta t_i^m - \min_{i=1,2,\ldots N_m} \Delta t_i^m \le \delta_t, \tag{38}$$

where δ_t is a specified tolerance for flight time step size.

To coordinate the flight time of different members, the lower-bound constraint of the time-step size is introduced to the individual optimization:

$$\begin{aligned} \Delta t_i^m &\ge \Delta t_{\min}^m, i = 1, 2, \ldots N_m \\ \Delta t_{\min}^m &= (\max_{j\in\Theta}(\Delta \bar{t}_j^m) + \min_{j\in\Theta}(\Delta \bar{t}_j^m))/2, \\ \Theta &= \{j \Big| \Big| \Delta \bar{t}_j^m - \Delta \bar{t}_j^{m-1} \Big| \Big/ \Delta \bar{t}_j^{m-1} \le \delta_{\Delta t}\}, \end{aligned} \tag{39}$$

where $\Delta t_{\min}^m$ is the lower bound of the time-step size and $\Delta \bar{t}_j^m$ is the time-step size of the nominal trajectory.

It may be noticed that when calculating $\Delta t_{\min}^m$, only the members whose variation of the nominal step size is less than the specified error, $\delta_{\Delta t}$, are considered.

Third, the cooperative constraints that have not been satisfied in the previous iteration are identified, and they will be considered in the next iteration of the SCP optimization. To identify the cooperative constraints that are required to be considered in the next iteration, a collision-avoidance safety factor, r_1, is defined, and the member pairs that have violated the distance $r_1 \cdot R_s$ in a previous iteration is identified. Thus, the collision-avoidance constraints may be expressed as follows:

$$\begin{aligned} &(\bar{\boldsymbol{x}}_i[k] - \bar{\boldsymbol{x}}_j[k])^T \cdot \boldsymbol{C}_1^T \boldsymbol{C}_1 \cdot (\boldsymbol{x}_i[k] - \bar{\boldsymbol{x}}_j[k])^T \\ &\quad \ge R_s \cdot \left\| \boldsymbol{C}_1 \cdot \bar{\boldsymbol{x}}_i[k] - \boldsymbol{C}_1 \cdot \bar{\boldsymbol{x}}_j[k] \right\| \\ &\qquad i = 1, 2, \ldots, N_m, \quad j < i,\ j \in \Gamma_i,\ k = 1, 2, \ldots, K, \end{aligned} \tag{40}$$

$$\begin{aligned} \Gamma_i = \{j | \exists k \in 1, 2, \ldots, K \text{ such that} \\ \times \left\| \boldsymbol{C}_1 \cdot [\bar{\boldsymbol{x}}_i[k] - \bar{\boldsymbol{x}}_j[k] \right\| < r_1 \cdot R_s\}. \end{aligned} \tag{41}$$

For the no-fly zone avoidance constraints, the no-fly zone avoidance safety factor, r_2, is defined. Only the members within the distance of $r_2 \cdot R_{n,l}$ from the center of the l^{th} no-fly zone in the previous iteration are required to avoid the no-fly zone in the next iteration. The no-fly zone avoidance constraints may be expressed as follows:

$$\begin{aligned} &\left\| \boldsymbol{C}_2 \cdot \bar{\boldsymbol{x}}_i[k] - \boldsymbol{p}_{nfz,l} \right\| \\ &\quad + \frac{(\boldsymbol{C}_2 \cdot \bar{\boldsymbol{x}}_i[k] - \boldsymbol{p}_{nfz,l})^T}{\left\| \boldsymbol{C}_2 \cdot \bar{\boldsymbol{x}}_i[k] - \boldsymbol{p}_{nfz,l} \right\|} \cdot (\boldsymbol{C}_2 \cdot \boldsymbol{x}_i[k] - \boldsymbol{C}_2 \cdot \bar{\boldsymbol{x}}_i[k]) \ge R_{n,l}, \end{aligned} \tag{42}$$

$$\begin{aligned} &\left\| \boldsymbol{C}_2 \cdot \bar{\boldsymbol{x}}_i[k-1] - \boldsymbol{p}_{nfz,l} \right\| \\ &\quad + \frac{(\boldsymbol{C}_2 \cdot \bar{\boldsymbol{x}}_i[k-1] - \boldsymbol{p}_{nfz,l})^T}{\left\| \boldsymbol{C}_2 \cdot \bar{\boldsymbol{x}}_i[k-1] - \boldsymbol{p}_{nfz,l} \right\|} \\ &\quad \cdot (\boldsymbol{C}_2 \cdot \boldsymbol{x}_i[k] - \boldsymbol{C}_2 \cdot \bar{\boldsymbol{x}}_i[k-1]) \ge R_{n,l} \\ &\quad i = 1, 2, \ldots, N_m, l \in \Lambda_i, k = 1, 2, \ldots, K \\ &\Lambda_i = \{l | \exists k \in 1, 2, \ldots, K \text{ such that} \\ &\quad \times \left\| \boldsymbol{C}_2 \cdot [\bar{\boldsymbol{x}}_i[k] - \boldsymbol{p}_{nfz,l}] \right\| < r_2 \cdot R_{n,l}\}. \end{aligned} \tag{43}$$

Similarly, the interceptor missile-avoidance safety factor, r_3, is defined. Only the members within the distance of $r_3 \cdot R_I$ from the n^{th} interceptor missile in the previous iteration are required to avoid the interceptor missile in the next iteration. The interceptor missile avoidance constraints may be written as follows:

$$\begin{aligned} &(\bar{\boldsymbol{x}}_i[k] - \boldsymbol{x}_{I,n}[k])^T \cdot \boldsymbol{C}_1^T \boldsymbol{C}_1 \cdot (\boldsymbol{x}_i[k] - \boldsymbol{x}_{I,n}[k])^T \\ &\quad \ge R_s \cdot \left\| \boldsymbol{C}_1 \cdot \bar{\boldsymbol{x}}_i[k] - \boldsymbol{C}_1 \cdot \boldsymbol{x}_{I,n}[k] \right\| \\ &\qquad i = 1, 2, \ldots, N_m, \quad n \in \Upsilon_i,\ k = 1, 2, \ldots, K, \end{aligned} \tag{44}$$

$$\begin{aligned} \Upsilon_i = \{n | \exists k \in 1, 2, \ldots, K \text{ such that} \\ \times \left\| \boldsymbol{C}_1 \cdot [\bar{\boldsymbol{x}}_i[k] - \boldsymbol{x}_{I,n}[k] \right\| < r_3 \cdot R_I\}. \end{aligned} \tag{45}$$

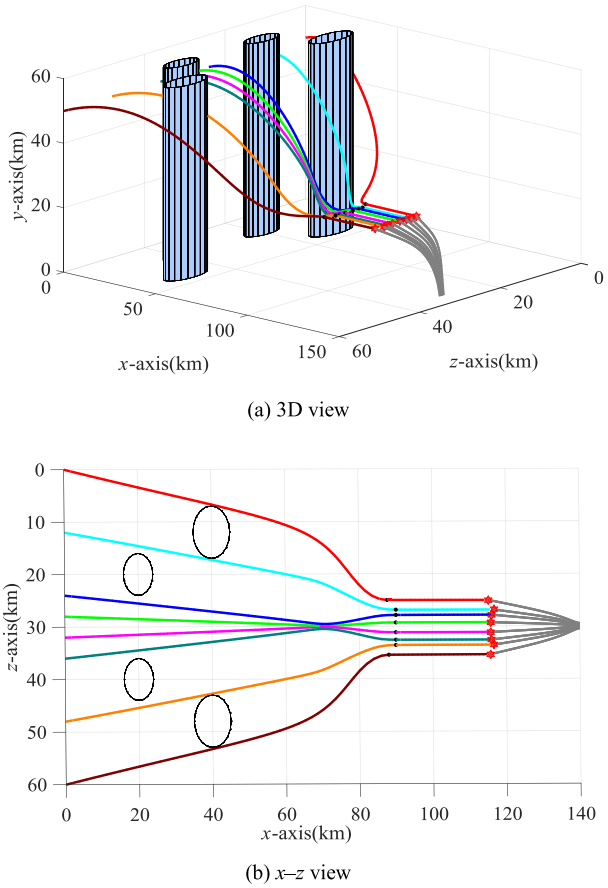

(a) 3D view

(b) x–z view

FIGURE 5. Members are successfully intercepted.

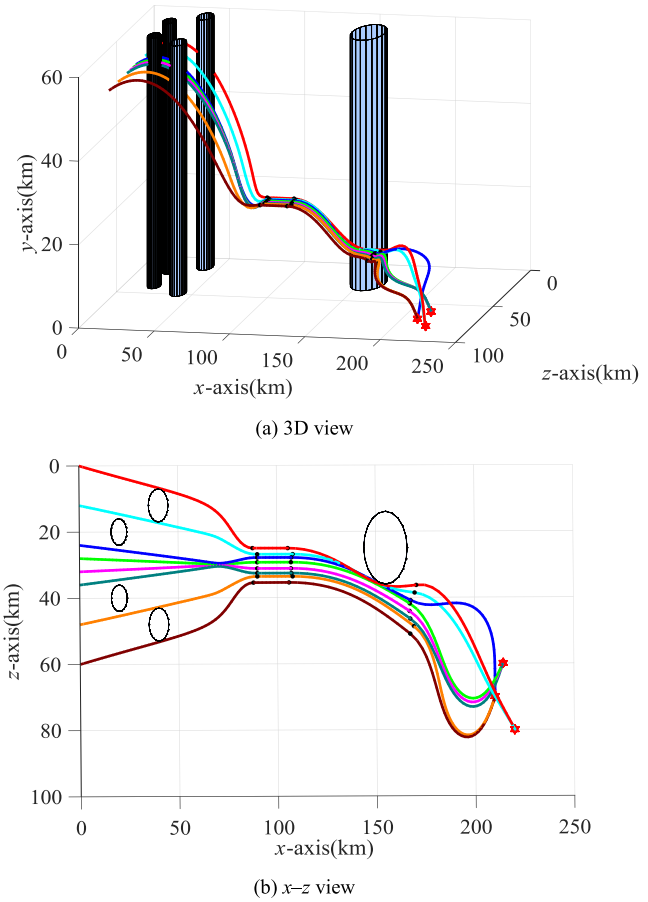

(a) 3D view

(b) x–z view

FIGURE 6. Planned trajectories by Bil-SCP (Case 1).

Cleary, the number of cooperative constraints in each iteration can be greatly reduced. Each member retained in the optimization sequence solves the trajectory optimization sub-problem in its individual level independently and sequentially, considering the identified cooperative constraints at the system level and the time-consensus constraint. Once one missile member completes its optimization, it will broadcast its current optimal trajectory to the remaining missile members in the optimization sequence. Thus, the trajectory optimization of other missiles can be performed in turn.

As the number of missiles participating in the optimization is gradually reduced with the evolution of iteration and the number of constraints considered is clearly decreased, the computational efficiency and the convergence property have been obviously improved for the cooperative trajectory optimization with the proposed Bil-SCP method, which is beneficial to the expansion of the formation size. To further improve the convergence property of SCP, at the individual level, the convex cooperative constraints have been gradually tightened up and have been included to the optimization with the evolution of optimization iteration of SCP, and thus to form a sequence of more relaxed and feasible intermediate optimization problems. The procedures at the system and individual levels will continue to be executed until the optimization sequence is empty, which would indicate that the Bil-SCP method for cooperative trajectory optimization has been completed.

Thus far, the multistage cooperative trajectory planning of multimissile formation has been described as the convex trajectory programming problem, $\mathbf{P}_4$:

$$\underset{i=1,2,\ldots N_m}{\text{Min}} \begin{cases} \sum_{i=1}^{N_m}\sum_{k=1}^{K}(u_{3i}\cdot\Delta t), & p=1,2,3 \\ -V_i(t_4)+c_\psi\int_{t_3}^{t_4}\psi_i \mathrm{d}t, & p=4 \end{cases}$$

$$\text{s.t.:} \begin{cases} (20)(24)(25)(29)(30)(35)(39)\sim(43), \\ \quad p=1,2; \\ (20)(24)(25)(29)(30)(35)(39)\sim(45), \\ \quad p=3; \\ (20)(24)(25)(29)(30)(35)(39)(42)(43), \\ \quad p=4. \end{cases} \tag{46}$$

For convenience, the elements in Γ_i, Λ_i, Υ_i have been arranged in ascending order of their sequence numbers.

Algorithm 1 Bi-Level SCP

$\{\bar{\boldsymbol{x}}_i; \bar{\boldsymbol{u}}_i; \Delta\bar{t}_i\}$ = initial guess, $\forall i$
$\Gamma_i, \Lambda_i, \Upsilon_i = \varnothing, \forall i$
$\{\boldsymbol{x}_i^0; \boldsymbol{u}_i^0; \Delta t_i^0\}$ =solution to $\mathbf{P}_4$ without Eqs. (39)(40)(42)(44), $\forall i$
$\bar{\boldsymbol{x}}_i = \boldsymbol{x}_i^0, \bar{\boldsymbol{u}}_i = \boldsymbol{u}_i^0, \Delta\bar{t}_i = \Delta t_i^0$
Update $\Gamma_i, \Lambda_i, \Upsilon_i$ using Eqs. (41)(43)(45), $\forall i$
$\Omega = \{1, 2, ...N_m\}$
$m = 1$
while $\Omega \neq \emptyset$
  for all $i \in \Omega$
    $\Delta t_{\min}^m = (\max(\Delta\bar{t}_j^m) + \min(\Delta\bar{t}_j^m))/2, j \in \Theta$
    N = the maximum element number of $\Gamma_i, \Lambda_i, \Upsilon_i$
    $Set\Gamma = \Gamma_i, Set\Lambda = \Lambda_i, Set\Upsilon = \Upsilon_i$
    $\Gamma_i, \Lambda_i, \Upsilon_i = \varnothing$
    for $s = 1, 2...N$
      $\Gamma_i = \Gamma_i \cup Set\Gamma(s), \Lambda_i = \Lambda_i \cup Set\Lambda(s), \Upsilon_i = \Upsilon_i \cup Set\Upsilon(s)$
      $\{\boldsymbol{x}_i^s; \boldsymbol{u}_i^s; \Delta t_i^s\}$ =solution to $\mathbf{P}_4$ with iteration s
      $\bar{\boldsymbol{x}}_i = \boldsymbol{x}_i^s, \bar{\boldsymbol{u}}_i = \boldsymbol{u}_i^s, \Delta\bar{t}_i = \Delta t_i^s$
    end for
    $\{\boldsymbol{x}_i^m; \boldsymbol{u}_i^m; \Delta t_i^m\} = \{\boldsymbol{x}_i^N; \boldsymbol{u}_i^N; \Delta t_i^N\}$ is the solution to $\mathbf{P}_4$ for member i
    Update $\Gamma_i, \Lambda_i, \Upsilon_i$ using Eqs. (21)(22)(23)
    $\bar{\boldsymbol{x}}_i = \boldsymbol{x}_i^m, \bar{\boldsymbol{u}}_i = \boldsymbol{u}_i^m, \Delta\bar{t}_i = \Delta t_i^m$
  end for
  if Eq.(38) is satisfied
    for all $i \in \Omega$
      if $\boldsymbol{x}_i^m$ satisfy Eqs. (21)(22)(23) and $\left|\boldsymbol{x}_i^m[k] - \boldsymbol{x}_i^{m-1}[k]\right| \leq \boldsymbol{\delta}$
        Remove i from Ω
      end if
    end for
  end if
  $m = m + 1$
end while
$\{\boldsymbol{x}_i^{m-1}; \boldsymbol{u}_i^{m-1}; \Delta t_i^{m-1}\}$ is the solution to $\mathbf{P}_4, \forall i$

An iteration parameter, s, of SCP has been defined; then, $\Gamma_i(s)$ is represented as a single-element set, containing only the s^{th} element of set Γ_i. If s is greater than the number of elements of Γ_i, then $\Gamma_i(s) = \varnothing$. Based on the aforementioned explanation, **Algorithm 1** provides the pseudocode of the proposed Bil-SCP method.

V. NUMERICAL SIMULATION

In this section, the Bil-SCP method is applied to solve the multistage cooperative trajectory planning problem for multimissile formation. The simulation is executed in a computer with an Intel core i7-4790@3.6GHz processor. The SCP method is implemented using the CVX toolbox with the solver SDPT3, and the solver uses the default settings. The parameters in the simulation cases are listed in Table 1.

TABLE 1. Parameters in simulation.

Symbol	N_m	g_0/(m/s^2)	S_{ref}/m^2	R_0/km	m_{ref}/kg
Value	8	9.8	0.292	6371	200
Symbol	$\tilde{\eta}$	$q_{\max}$/(kN/m^2)	$n_{\max}$	R_s/m	R_f/m
Value	3	100	15	150	400
Symbol	R_d/km	r_1	r_2	r_3	
Value	20	1.5	1.5	1.5	

The constraints for states and controls are

$$\begin{aligned}\boldsymbol{x}_{i\min} &= [\frac{0}{\sqrt{g_0R_0}} \frac{-\pi}{2} \frac{-\pi}{2} \frac{0e3}{R_0} \frac{0e3}{R_0} \frac{0e3}{R_0}]\\ \boldsymbol{x}_{i\max} &= [\frac{1200}{\sqrt{g_0R_0}} \frac{\pi}{2} \frac{\pi}{2} \frac{100e3}{R_0} \frac{60e3}{R_0} \frac{100e3}{R_0}]\\ \boldsymbol{u}_{i\min} &= [-3\ -30], \quad \boldsymbol{u}_{i\max} = [33\ 9].\end{aligned} \tag{47}$$

Let

$$\boldsymbol{\varepsilon} = [\frac{200}{\sqrt{g_0R_0}} \frac{50\pi}{180} \frac{50\pi}{180} \frac{10e3}{R_0} \frac{10e3}{R_0} \frac{10e3}{R_0}]. \tag{48}$$

The iterative convergence tolerance vector is

$$\boldsymbol{\delta} = [\frac{2}{\sqrt{g_0R_0}} \frac{\pi}{180} \frac{\pi}{180} \frac{50}{R_0} \frac{50}{R_0} \frac{50}{R_0}]. \tag{49}$$

The specified tolerances for flight time step size are $\delta_t = 0.01$s and $c_\psi = 0.01$.

To explore the robustness and stability of the proposed method, two cases with different initial/final positions of each member and target, and boundary constraint values are considered. In Case 1, the missiles are aggregated from the initial positions firstly, as listed in Table 2, to form the formation of the specified positions listed in Table 4. Then, the members continue flying in formation; the missiles immediately initiate maneuvering avoidance, once a member detects the interceptor missiles. After all the formation members have successfully penetrated the interceptor missiles, the genetic method is employed to construct the optimal target allocation model, according to the geometric advantage of the position of each member to each target. Three ground targets that are located at (210,0,70), (214,0,60), and (220,0,80) km are attacked, and each target is attacked by at least two members simultaneously, to ensure the greatest damage effect. The initial position of each member and the final position allocated by the target assignment model are listed in Table 2. The positions and the radii of the no-fly zones are summarized in Table 3. The initial nominal trajectory for each member is selected as the straight line connecting its specified initial and final positions. The number of discrete points in each stage is set as 50, 10, 20, and 30.

In the simulation of Case 1, when the members have been aggregated, eight interceptor missiles are immediately launched from the ground with the x-axis coordinate of 140km, with a common launch angle of 80° to intercept each member of the formation according to the proportional guidance law. If the formation does not take the maneuvering avoidance, each member will be successfully intercepted,

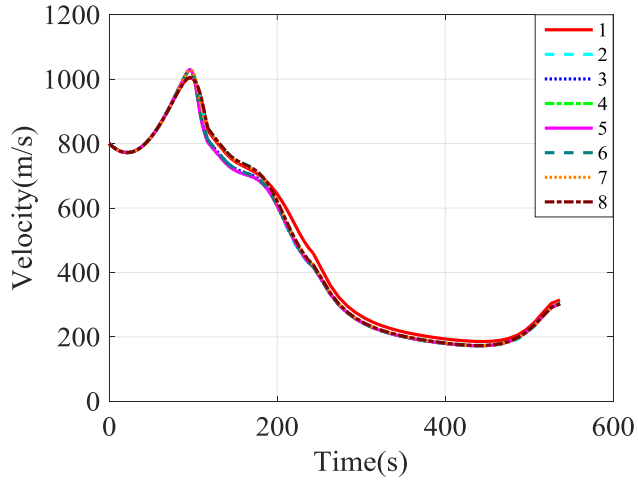

(a) Velocity

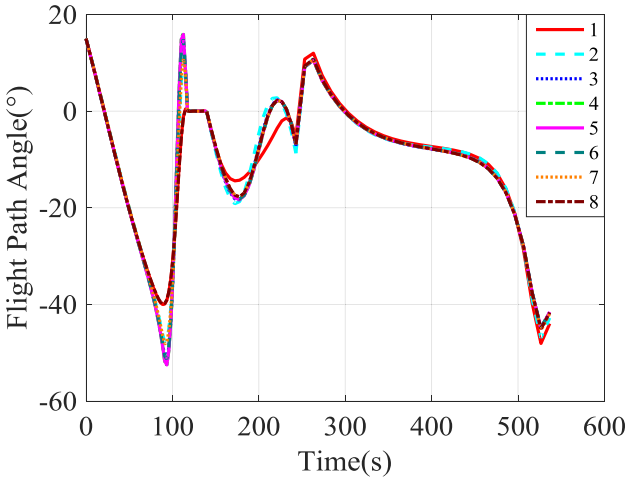

(b) Flight path angle

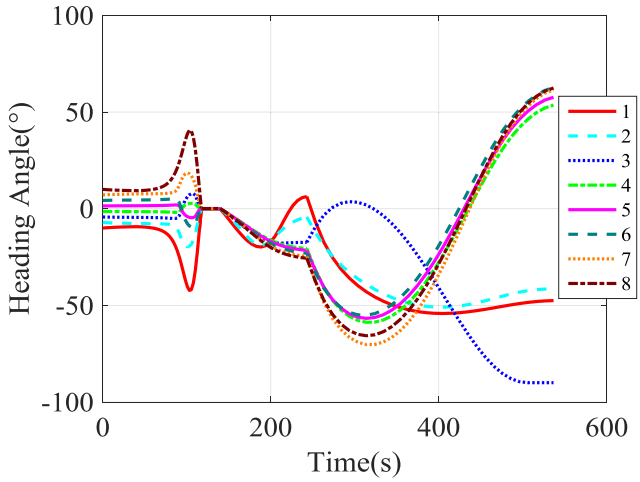

(c) Heading angle

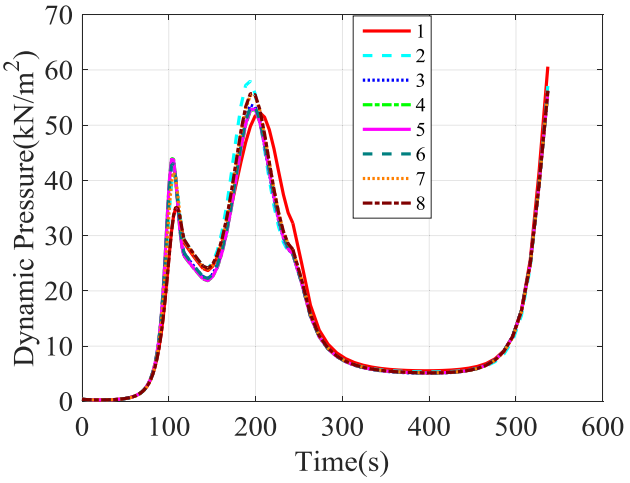

(d) Dynamic pressure

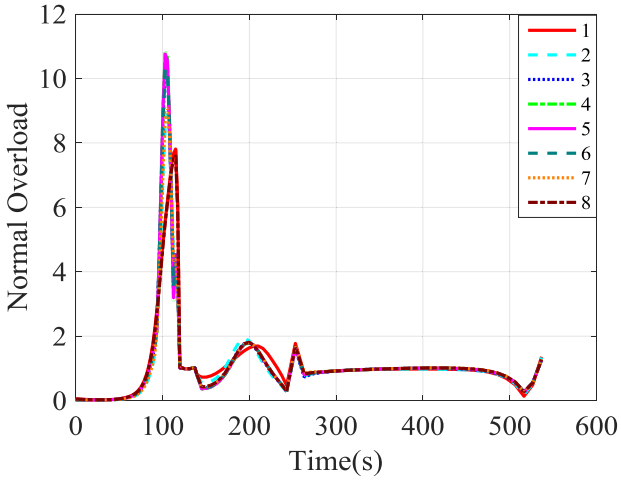

(e) Normal overload

FIGURE 7. Optimized flight states of all members (Case 1).

as shown in Fig. 5. To avoid interceptor missiles, the formation proceed to initiate maneuvering avoidance once a member detect the interceptor missile within the detection range, R_d. The multistage cooperative trajectory optimization is solved by using the proposed Bil-SCP method, and the obtained optimal trajectories for the formulation are

TABLE 2. Initial position and final position of each member and target allocated (Case 1).

Member number	Initial position/km	Final position/km
1	(0,50,0)	(220,0,80)
2	(0,50,12)	(220,0,80)
3	(0,50,24)	(210,0,70)
4	(0,50,28)	(214,0,60)
5	(0,50,32)	(214,0,60)
6	(0,50,36)	(214,0,60)
7	(0,50,48)	(210,0,70)
8	(0,50,60)	(210,0,70)

TABLE 3. Positions and radii of the no-fly zones.

No-fly zone number	Position/km	Radius/km
1	(40,0,12)	5
2	(40,0,48)	5
3	(20,0,20)	4
4	(20,0,40)	4
5	(155,0,25)	11

TABLE 4. Boundary constraints (Case 1).

Stages	Boundary constraints	Stage	Boundary constraints
1	$V_{i,t_0}=800\text{m/s}$ $\theta_{i,t_0}=15°$ $-10°\le\psi_{i,t_0}\le10°$ $\theta_{i,t_1}=0°$ $\psi_{i,t_1}=0°$ $85\text{km}\le x_{i,t_1}\le90\text{km}$ $19.5\text{km}\le y_{i,t_1}\le20.5\text{km}$ $25\text{km}\le z_{i,t_1}\le35\text{km}$	2	$-0.1°\le\theta_{i,t_2}\le0.1°$ $-0.4°\le\psi_{i,t_2}\le0.4°$ $19.5\text{km}\le y_{i,t_2}\le20.5\text{km}$ $25\text{km}\le z_{i,t_2}\le35\text{km}$
3	$30\text{km}\le z_{i,t_3}\le50\text{km}$ $10\text{km}\le y_{i,t_3}\le12\text{km}$	4	$\theta_{i,t_4}\le-40°$

TABLE 5. Final time of each stage (Case 1).

Final time	t_1	t_2	t_3	t_4
Value	117.1s	139.2s	242.5s	536.3s

illustrated in Fig. 6, in which the junctions between the adjacent stages are marked as black dots. It is obvious that the formation is successfully aggregated to the specified altitude, as listed in Table 4. After the maintenance stage of the formation, maneuvering avoidance is performed. Once the missiles avoided the interception of the interceptor missiles, the targets are successfully attacked and the no-fly zones are successfully avoided as well. The trajectories could obviously consider the different task requirements of each stage, and the trajectory connections between the adjacent stages are continuous and smooth.

The final time of each stage is listed in Table 5, which reveals that each stage has a free flight time.

The optimal states of all eight members of Case 1 are shown in Fig. 7, from which it is observed that the states of the members all satisfy the state constraints. From Fig. 7 (a), it is observed that the velocity increases gradually at the end

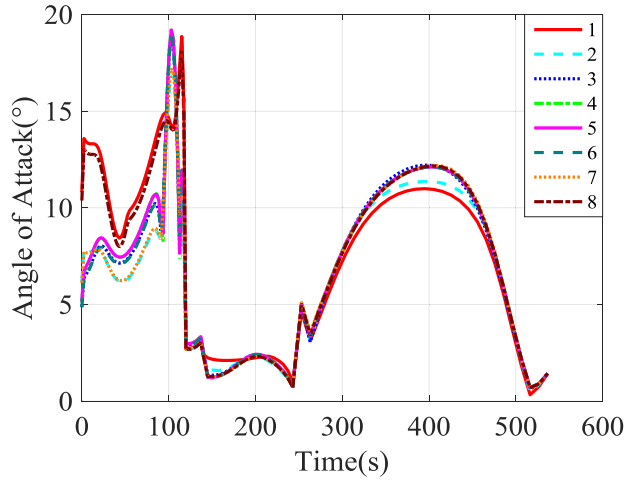

(a) Angle of attack

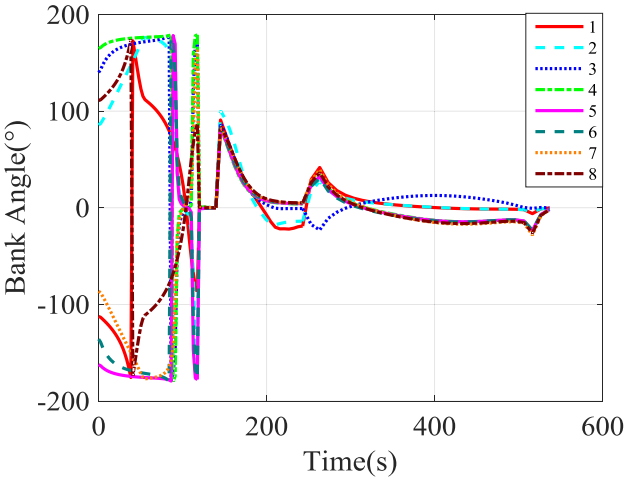

(b) Bank angle

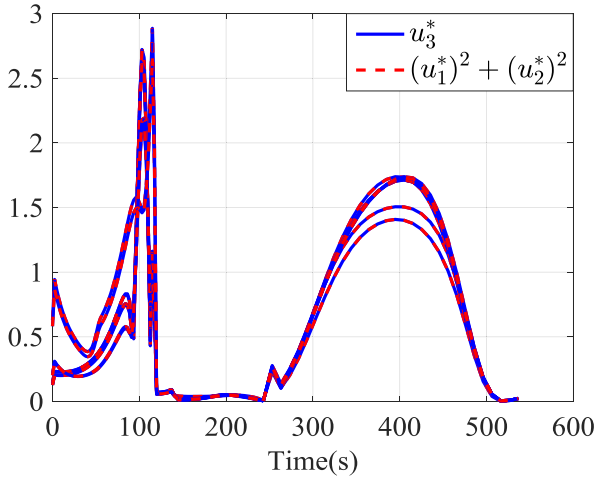

(c) $(u_1^*)^2+(u_2^*)^2$ and u_3^*

FIGURE 8. Optimal controls of all members (Case 1).

of the flight to achieve the maximum-velocity attack on the targets. The path constraints of the dynamic pressure and normal overload are also satisfied.

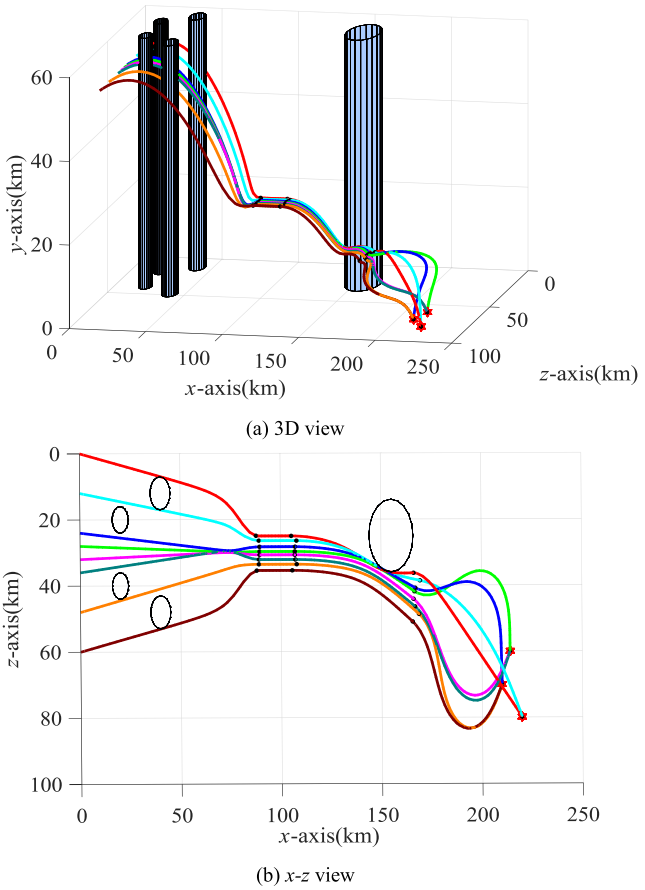

FIGURE 9. Optimal trajectories by GPOPS (Case 1).

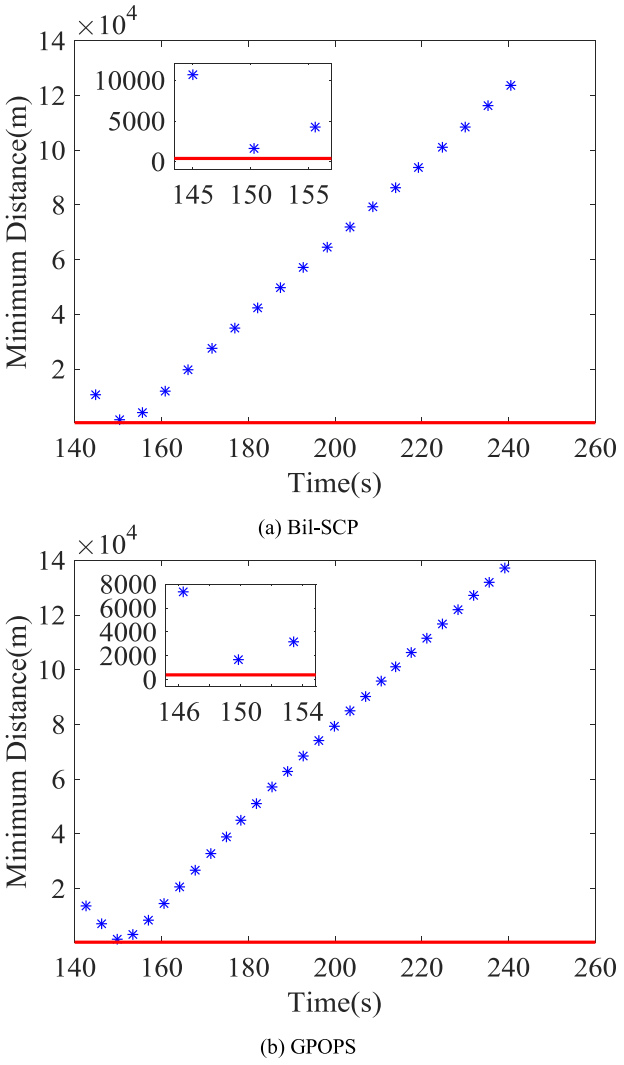

FIGURE 10. Minimum distance between missile members and interceptor missiles (Case 1).

The obtained optimal controls of Case 1 are shown in Fig. 8. From Figs. 8(a) and (b), at the early stage of formation aggregation (0s to 117.1 s), the magnitude of the bank angle of the members are greater than 90°; therefore, negative lift is produced to reduce the flight height of the members with the purpose of aggregating to the designated airspace. At a later stage of formation aggregation, the angles of attack decrease and the bank angles gradually converge to 0° to satisfy the boundary constraints of the flight path angle and heading angle, as listed in Table 4. At the formation maintenance stage (117.1s to 139.2 s), only slight lateral maneuvers are required. Therefore, the bank angle is 0° each, and the angles of attack are small for the mere purpose of maintaining the flight altitude. Once entering the formation penetration stage (139.2s to 242.5s), the bank angles rapidly increase to generate rapid lateral maneuvers to avoid interceptor missiles. At the cooperative attack stage (242.5s to 536.3 s), the angles of attack gradually increase to first generate positive lift to increase the flight height of the members; and thus, the maximum velocity of attack on the targets can be achieved.

Fig. 8(c) shows that constraints $(u_{1i}^*)^2 + (u_{2i}^*)^2 = u_{3i}^*$ of all members are valid within $[t_0, t_4]$, which indicates that **Lemma 1** has been proven. Therefore, $\mathbf{P}_4$ realizes the exact convex relaxation to $\mathbf{P}_2$; the optimal solution of $\mathbf{P}_4$ is the approximate optimal solution of problem $\mathbf{P}_1$.

To investigate the efficiency of the proposed Bil-SCP method, the Gauss pseudospectral method implemented in the generation optimal control software (GPOPS) toolbox is also employed to solve the cooperative trajectory optimization problem with the same simulation scenario and constraints. Here, the Gauss pseudospectral method is used at the individual level as a replacement of the SCP to solve the trajectory optimization sub-problems for all members, sequentially. At the system level, there is no detection of cooperative constraints. The number of discrete points at each stage is set as the same to that of the Bil-SCP. The optimal trajectories obtained by GPOPS are shown in Fig. 9. It can be seen that the formation is successfully aggregated to the specified altitude, as listed in Table 4. After the formation maintenance stage, maneuvering avoidance is performed to avoid the interception of the interceptor missiles. The targets

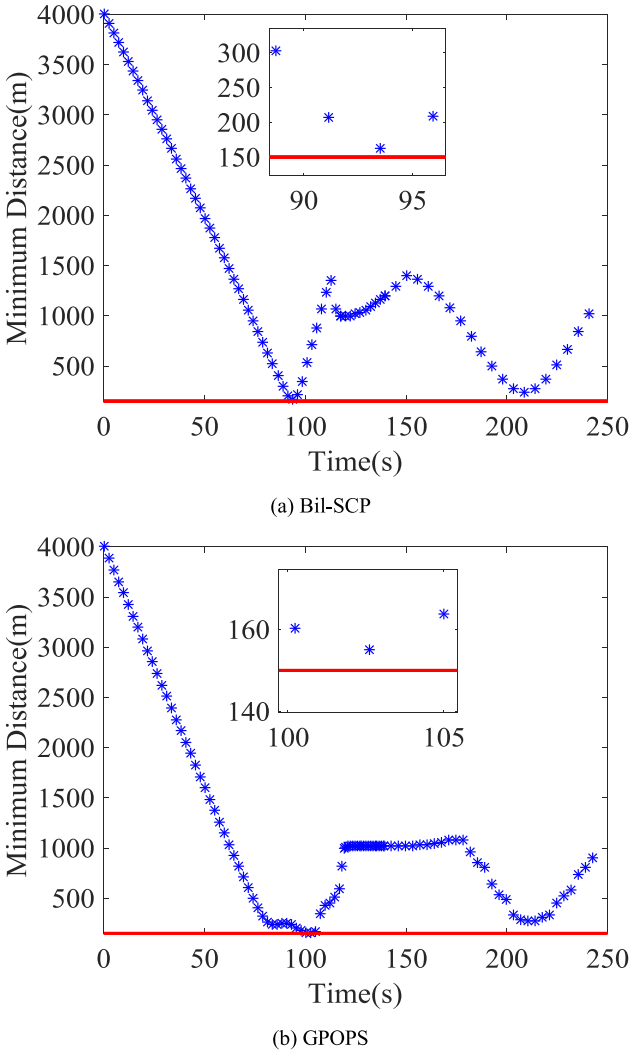

(a) Bil-SCP

(b) GPOPS

FIGURE 11. Minimum distance between members (Case 1).

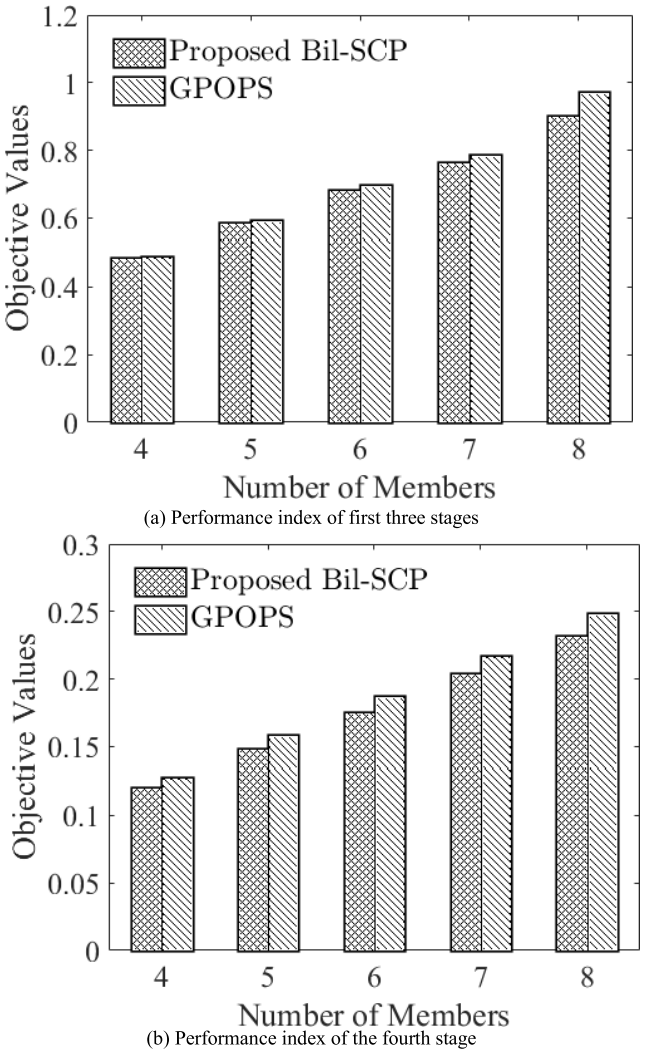

(a) Performance index of first three stages

(b) Performance index of the fourth stage

FIGURE 12. Performance index of different methods (Case 1).

are successfully attacked and the no-fly zones are successfully avoided as well.

To clearly show that whether the interceptor missiles avoidance constraints and the collision-avoidance constraints have been satisfied for Bil-SCP and GPOPS, the minimum distance between the missile members and the interceptor missiles at the penetration stage and the minimum distance between the missile members at the first three flight stages are shown in Figs. 10 and 11, respectively. It may be noticed that both types of minimum distances are always above the lower bounds (depicted by the red solid line). These results demonstrate the effectiveness of the proposed Bil-SCP method and the GPOPS in solving multimissile formation cooperative trajectory planning problems.

To further investigate the advantage in the efficiency of the proposed method, simulations with different number of missile members ($N_m = 4, 5, 6, 7, 8$) are conducted for Bil-SCP and GPOPS. The dimensionless optimal performance index of the first three stages, i.e., $(\sum_{i=1}^{N_m} \int_{t_0}^{t_3} u_{3i} \mathrm{d}t)$ and the magnitude of the dimensionless optimal performance index of the fourth stage, i.e., $(V_i(t_4))$, of the two methods are shown in Figs. 12 (a) (b), respectively. As can be seen from Fig. 12, the optimal performance indices produced by each of the two methods are remarkably close to one another. The maximum difference (Fig. 12(a), eight members) is approximately 8%, and the difference in most simulation scenarios is approximately 6%. These results further demonstrate the effectiveness of the proposed Bil-SCP method for cooperative trajectory planning.

The computational time of Bil-SCP and GPOPS is compared and is shown in Fig. 13. It can be seen that with the increase in the formation size (N_m), the computational time of Bil-SCP and GPOPS increases approximately linearly and exponentially, respectively. Clearly, Bil-SCP is significantly more efficient than GPOPS, which becomes more obvious with the increase in formation size. The gain in the efficiency of Bil-SCP is attributed to the employment of the highly efficient SCP. The average computational time for each optimization iteration in SCP of Bil-SCP is shown in Fig. 14.

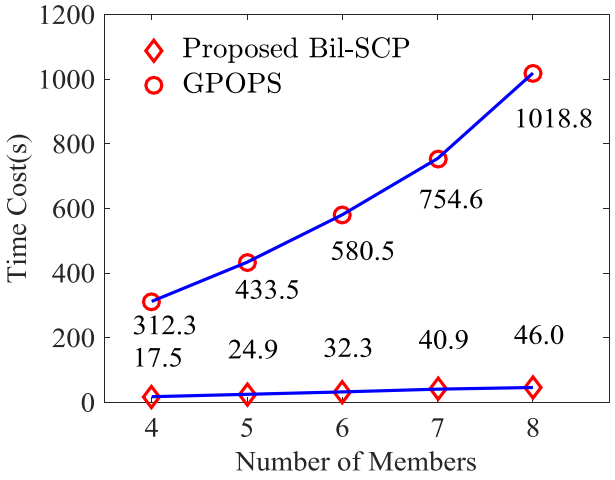

FIGURE 13. Time cost.

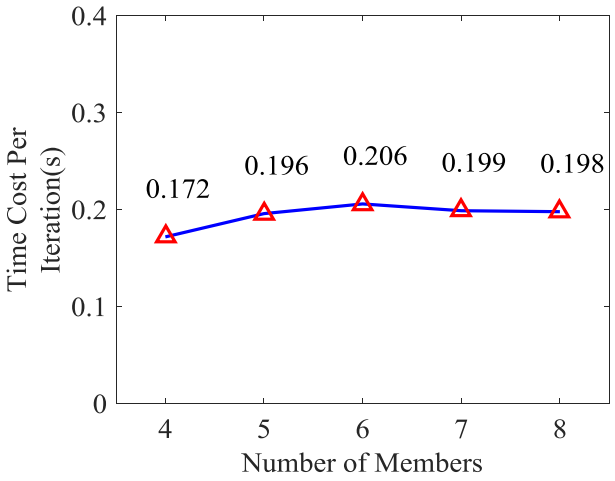

FIGURE 14. Time cost per iteration of Bil-SCP (Case 1).

Member number

Iterations	1	2	3	4	5	6	7	8
1	2.4329	2.2784	2.2791	2.2774	2.2838	2.2971	2.3011	2.3552
2	2.4159	2.3467	2.3467	2.3499	2.3565	2.3585	2.3813	2.4166
3	2.4093	2.3816	2.3832	2.3866	2.3876	2.3990	2.3991	2.3955
4	2.4035	2.3934	2.3950	2.3955	2.3984	2.3984	2.3984	2.3984
5	2.3987	2.3968	2.3971	2.3978	2.3978	2.3978	2.3978	2.3978
6	2.3974	2.3974	2.3976	2.3976	2.3976	2.3976	0	0
7	2.3978	2.3976	2.3977	0	2.3977	0	0	0
8	0	0	0	0	2.3977	0	0	0
9	0	0	0	0	0	0	0	0
10	0	0	0	0	0	0	0	0

FIGURE 15. Convergence process at the formation aggregation stage with exclusion strategy (Case 1).

Member number

Iterations	1	2	3	4	5	6	7	8
1	2.4329	2.2784	2.2791	2.2774	2.2838	2.2971	2.3011	2.3552
2	2.4159	2.3467	2.3467	2.3499	2.3565	2.3585	2.3813	2.4166
3	2.4093	2.3816	2.3832	2.3866	2.3876	2.3990	2.3991	2.3955
4	2.4035	2.3934	2.3950	2.3955	2.3984	2.3984	2.3984	2.3984
5	2.3987	2.3968	2.3971	2.3978	2.3978	2.3978	2.3978	2.3978
6	2.3974	2.3974	2.3976	2.3976	2.3976	2.3976	2.3976	2.3975
7	2.3978	2.3976	2.3976	2.3976	2.3976	2.3976	2.3976	2.3977
8	0	0	0	0	0	0	0	0
9	0	0	0	0	0	0	0	0
10	0	0	0	0	0	0	0	0

FIGURE 16. Convergence process at the formation aggregation stage without exclusion strategy (Case 1).

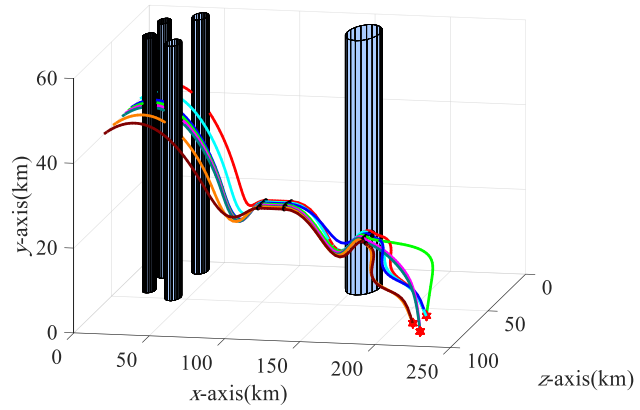

(a) 3D view

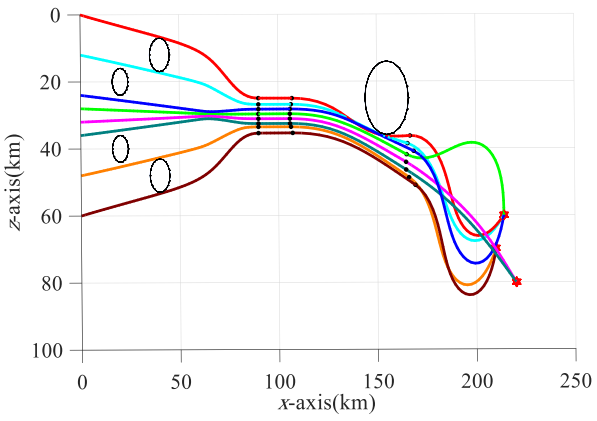

(b) x–z view

FIGURE 17. Planned trajectories by Bil-SCP (Case 2).

It can be seen that the average computational time is almost the same with that of a different formation size, which indicates that the increase in computational time is caused by the increase in the number of members. The interpretation is that with the increase in the number of members, more iterations are required by Bil-SCP; and thus, a higher computational cost is required. These results indicate that the proposed Bil-SCP method has good adaptability to the expansion of the formation size.

The proposed Bil-SCP method applies the exclusion strategy: when the flight time consensus constraint of the formation is satisfied, the members who have completed the trajectory optimization are removed from the optimization sequence. In order to test whether the exclusion strategy has an impact on the solution of consistent flight time, a contrast

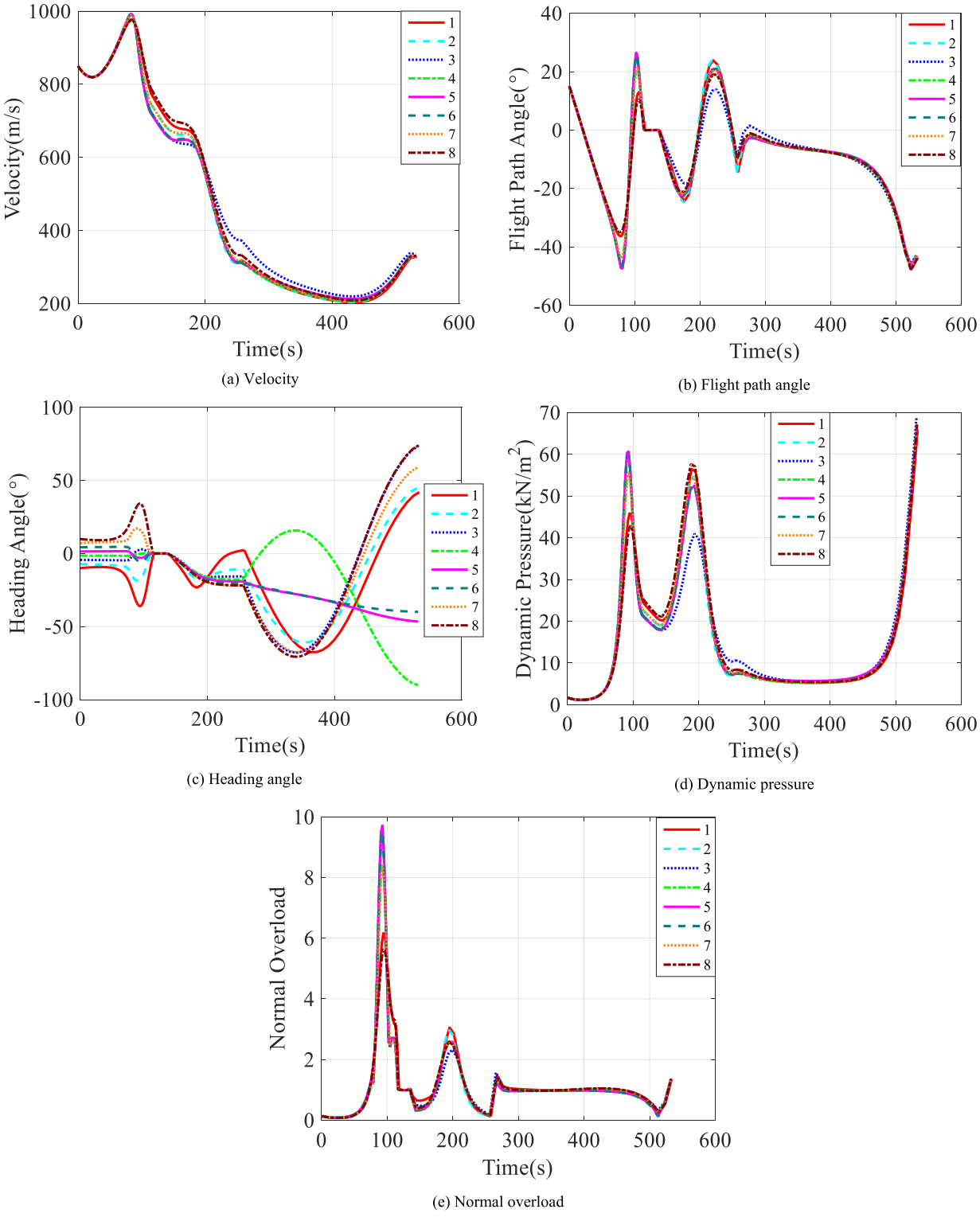

FIGURE 18. **Optimized flight states of all members (Case 2).**

simulation of Bil-SCP method without exclusion strategy is performed at the formation aggregation stage of Case 1.

The numerical matrix of members' flight time step size in the iterative process is established to observe the convergence process. And the numerical matrix of the two methods with or without the exclusion strategy are shown in Fig. 15 and Fig. 16, respectively. The horizontal axis represents the member number, and the vertical axis represents the number of iterations. Each non-zero value in the matrix represents the missile's flight time step solved by a convex optimization in

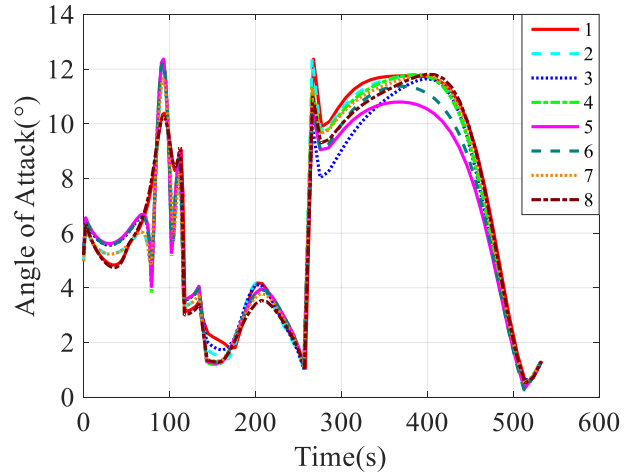

(a) Angle of attack

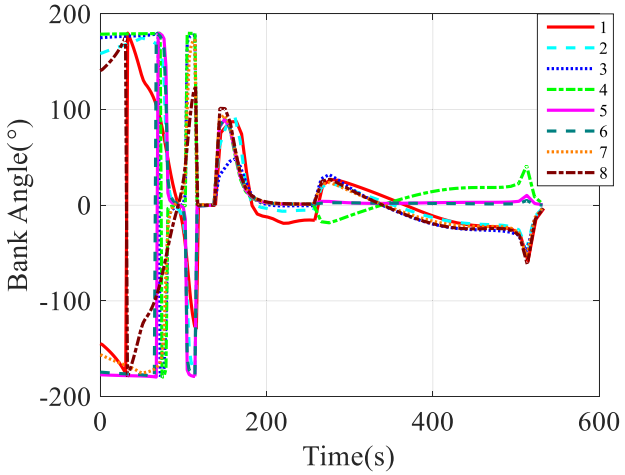

(b) Bank angle

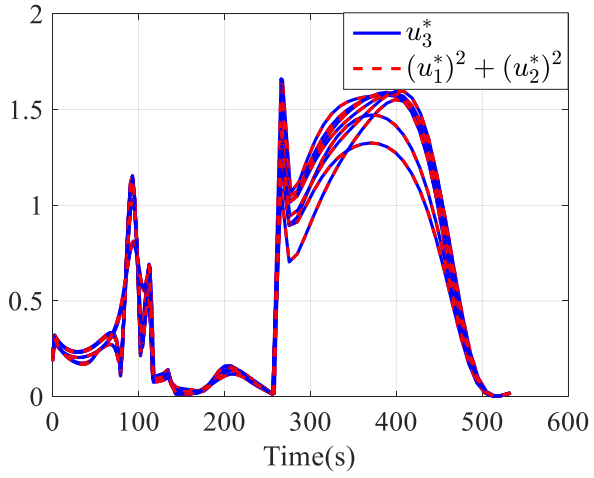

(c) $(u_1^*)^2 + (u_2^*)^2$ and u_3^*

FIGURE 19. Optimal controls of all members (Case 2).

the iterative process. Zero in the matrix means that the missile has converged to get the optimal trajectory. The values in the red boxes are the flight time step of the missiles' convergent solutions.

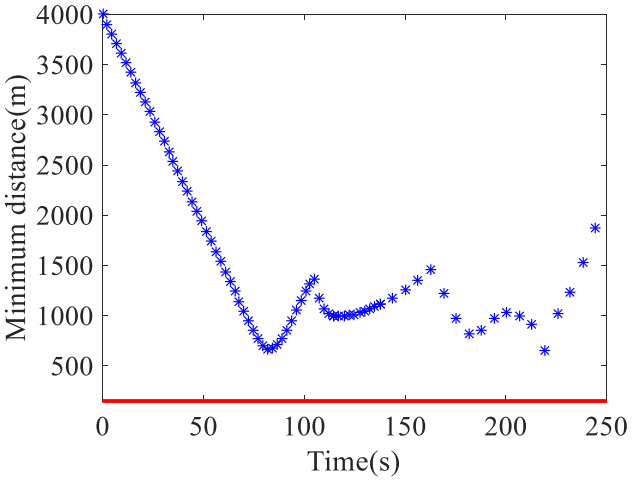

(a) Bil-SCP

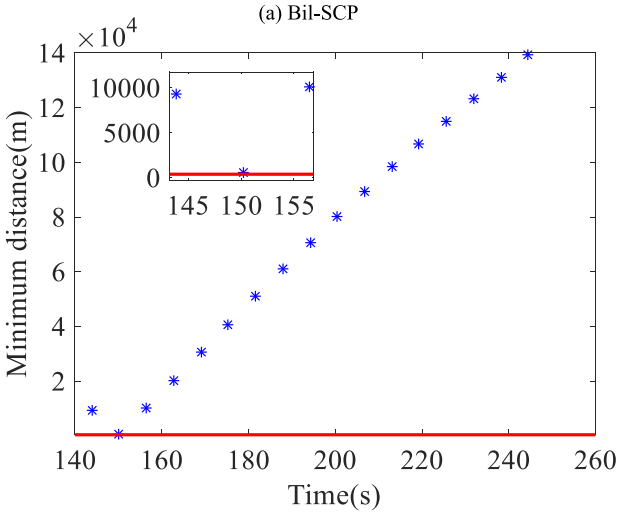

(b) GPOPS

FIGURE 20. Minimum distance between missile members and interceptor missiles (Case 2).

It can be seen from Fig. 15 that starting from the 6th iteration, some converged missile members are excluded from the optimization sequence, and after 8 iterations, the optimal solution of the formation is obtained, and a total of 51 convex optimization solutions are performed. Fig. 15 also shows that the flight time step of each missile's converged solution is within [2.3976, 2.3978] seconds, obviously satisfying the flight time consensus constraint shown in Eq. (38). Fig. 16 shows the convergence process without the exclusion strategy. As can be seen from the figure, after 7 iterations, the optimal solution of the formation is obtained, and a total of 56 convex optimization solutions are performed, which is more than 51 times when the exclusion strategy is applied. The flight time step size of each missile's optimal solution is within [2.3976, 2.3978] seconds, which obviously satisfies the flight time consensus constraint shown in Eq. (38) and is the same with the flight time step obtained by using the exclusion strategy. According to the comparison simulation above, it can be seen that applying the exclusion strategy in the Bil-SCP method does not affect the optimization of the

TABLE 6. Initial position and final position of each member and target allocated (Case 2).

Member number	Initial position/km	Final position/km
1	(0,40,0)	(214,0,60)
2	(0,40,12)	(214,0,60)
3	(0,40,24)	(214,0,60)
4	(0,40,28)	(214,0,60)
5	(0,40,32)	(220,0,80)
6	(0,40,36)	(220,0,80)
7	(0,40,48)	(210,0,70)
8	(0,40,60)	(210,0,70)

TABLE 7. Boundary constraints (Case 2).

Stages	Boundary constraints	Stage	Boundary constraints
1	$V_{i,t_0}=850\text{m/s}$ $\theta_{i,t_0}=15°$ $-10°\le\psi_{i,t_0}\le10°$ $\theta_{i,t_1}=0°$ $\psi_{i,t_1}=0°$ $85\text{km}\le x_{i,t_1}\le90\text{km}$ $19.5\text{km}\le y_{i,t_1}\le20.5\text{km}$ $25\text{km}\le z_{i,t_1}\le35\text{km}$	2	$-0.1°\le\theta_{i,t_2}\le0.1°$ $-0.4°\le\psi_{i,t_2}\le0.4°$ $19.5\text{km}\le y_{i,t_2}\le20.5\text{km}$ $25\text{km}\le z_{i,t_2}\le35\text{km}$
3	$30\text{km}\le z_{i,t_3}\le50\text{km}$ $15\text{km}\le y_{i,t_3}$	4	$\theta_{i,t_4}\le-40°$

consistent flight time. And the Bil-SCP method using the exclusion strategy can obtain the same solution with lower computational cost, which is beneficial to the expansion of formation size.

To verify the adaptability of the proposed method to different constraints [27], in Case 2, the initial positions of all the missiles and the corresponding assigned targets are as shown in Table 6, and the boundary constraints of each flight stage are as shown in Table 7. Other simulation parameters are consistent with those of Case 1.

The obtained optimal trajectories for the formulation in Case 2 are illustrated in Fig. 17. It is obvious that the formation is successfully aggregated to the specified altitude, as listed in Table 7. And the targets are successfully attacked and the no-fly zones are successfully avoided as well.

The optimized states of all eight members in Case 2 are shown in Fig. 18, from which it is observed that the states of the members all satisfy the state constraints. Meanwhile, the path constraints of the dynamic pressure and normal overload are also satisfied.

The obtained optimal controls in Case 2 are shown in Fig. 19, from which it is observed that the control constraints are satisfied, and $(u_{1i}^*)^2+(u_{2i}^*)^2=u_{3i}^*$ of all members are valid within $[t_0,t_4]$, indicating that **Lemma 1** has also been proven in Case 2. Fig. 20 clearly shows that the interceptor missiles avoidance constraints and the collision-avoidance constraints have been satisfied for Bil-SCP in Case 2, which demonstrates the effectiveness of the proposed Bil-SCP method in solving multimissile formation cooperative trajectory planning problems.

The simulation results of Case 1 and Case 2 show that under different initial conditions and boundary constraints, the proposed Bil-SCP method can achieve the target attack and meet the given state constraints, and constraints on the dynamic pressure and overload are also satisfied, which indicates that the Bil-SCP method has robustness and can solve multistage cooperative trajectory planning problem of multimissile formation under different conditions and constraints.

VI. CONCLUSION

To improve the convergence property and computational efficiency, a Bil-SCP method is developed to solve the multistage cooperative trajectory planning of multimissile formation considering multiple complex constraints; meanwhile, the efficient sequential convex programming technique is extended. By decomposing the multistage cooperative trajectory planning problem to a system coordination level and an individual SCP-based trajectory optimization level, the convergence property and computational efficiency could greatly improve, and this is beneficial to the extension of the formation size. The results of two numerical simulations showed that the proposed method could generate effective optimal trajectories with good convergence property, high computational efficiency, and robustness, and good scalability to formation size; and it is shown that it is significantly more efficient than the GPOPS-based approach. The proposed Bil-SCP method has great application prospects in trajectory planning of large-scale multimissile formation.

APPENDIX
PROOF OF LEMMA 1

Firstly, we prove Lemma1 when the performance index is $-V(t_4)+c_\psi\int_{t_3}^{t_4}\psi\,\mathrm{d}t$:

The necessary optimality conditions of problem are introduced. Applying the maximum principle yields the following Hamiltonian H. Define the Hamiltonian and Lagrangian as

$$\begin{aligned}H=&\,p_v(a_{11}V+a_{12}\theta+a_{15}y+b_{13}u_3+c_1)\\&+p_\theta(a_{21}V+a_{22}\theta+a_{25}y+b_{21}u_1+c_2)\\&+p_\psi(a_{31}V+a_{32}\theta+a_{35}y+b_{32}u_2+c_3)\\&+p_x(a_{41}V+a_{42}\theta+a_{43}\psi+c_4)+p_y(a_{51}V+a_{52}\theta+c_5)\\&+p_z(a_{61}V+a_{62}\theta+a_{63}\psi+c_6)+p_0c_\psi\psi\end{aligned}\tag{50}$$

$$\begin{aligned}L=&\,H+\mu_u(u_3-u_1^2-u_2^2)+\mu_3^-u_3\\&+\mu_3^+(\tilde{u}_3-u_3)+\mu_v(\tilde{V}-V)\end{aligned}\tag{51}$$

where a_{ij}, b_{ij},and c_i are the nonzero elements in $\boldsymbol{A}(\boldsymbol{x}^m)$, $\boldsymbol{B}(\boldsymbol{x}^m)$, and $\boldsymbol{c}(\boldsymbol{x}^m)$, respectively; $\boldsymbol{p}=[p_vp_\theta p_\psi p_xp_yp_z]^T\in\boldsymbol{R}^6$ is the costate vector; and μ_u, μ_3^-, μ_3^+ and μ_v are the Lagrangian multipliers. According to the direct adjoining approach in optimal control theory, a constant $p_0\le0$ exists such that the following necessary optimality conditions hold for $\{\boldsymbol{x}^*,\boldsymbol{u}^*\}$:

1) The nontriviality condition

$$[p_0 \, \boldsymbol{p}^T \, \mu_v]^T \neq 0 \tag{52}$$

2) The costate equations

$$\begin{aligned} p'_v &= -\partial_v L = -a_{11}p_v - a_{21}p_\theta - a_{31}p_\psi \\ &\quad - a_{41}p_x - a_{51}p_y - a_{61}p_z + \mu_v \qquad (53) \\ p'_\theta &= -\partial_\theta L = -a_{12}p_v - a_{22}p_\theta - a_{32}p_\psi \\ &\quad - a_{42}p_x - a_{52}p_y - a_{62}p_z \qquad (54) \\ p'_\psi &= -\partial_\psi L = -a_{43}p_x - a_{63}p_z - c_\psi p_0 \qquad (55) \\ p'_x &= -\partial_x L = 0 \qquad (56) \\ p'_y &= -\partial_y L = -a_{15}p_v - a_{25}p_\theta - a_{35}p_\psi \qquad (57) \\ p'_z &= -\partial_z L = 0 \qquad (58) \end{aligned}$$

3) The stationary conditions

$$\begin{aligned} \partial_{u1} L &= p_\theta b_{21} - 2\mu_u u_1 = 0 \qquad (59) \\ \partial_{u2} L &= p_\psi b_{32} - 2\mu_u u_2 = 0 \qquad (60) \\ \partial_{u3} L &= p_v b_{13} + \mu_u + \mu_3^- - \mu_3^+ = 0 \qquad (61) \end{aligned}$$

4) The complementary slack conditions

$$\begin{aligned} \mu_u \geq 0, \quad \mu_u[u_3^* - (u_1^*)^2 - (u_2^*)^2] = 0 \qquad (62) \\ \mu_3^-, \quad \mu_3^+ \geq 0, \ \mu_3^- u_3^* = 0, \ \mu_3^+(\tilde{u}_3 - u_3^*) = 0 \qquad (63) \\ \mu_v \geq 0, \quad \mu_v(\tilde{V} - V^*) = 0 \qquad (64) \end{aligned}$$

5) The transversality conditions

$$p_v(t_4) = p_0 - \lambda_f \tag{65}$$

where $\lambda_f \geq 0$ is a constant and satisfies

$$\lambda_f[\tilde{V}(t_4) - V^*(t_4)] = 0 \tag{66}$$

Now we prove by counter-evidence. Specifically, suppose that there exists a finite interval $[t_a, t_b] \subset [t_3, t_4]$ where holds for $[u_1^*(t)]^2 + [u_2^*(t)]^2 < u_3^*(t)$. We will then attempt to counteract (52) in the following.

Under the supposition above, (62) implies $\mu_u = 0$, which can be substituted into (59) and (60) to get $p_\theta = p_\psi = 0$ whenever $u_1, u_2 \neq 0$ (note that $b_{21}, b_{32} \neq 0$). When $p_\psi = 0$, (55) becomes

$$p_0 = (-a_{43}p_x - a_{63}p_z)/c_\psi \tag{67}$$

It can be seen from (67) that p_0 (which is a constant) cannot be a constant unless p_x and p_z are all zero. Hence, (67) implies that

$$p_x = p_z = p_0 = 0 \tag{68}$$

Substituting (68) into (54)(57), and we can get $p_v = p_y = 0 (a_{15}, a_{52}, a_{12}$ are time-variant), thus $\boldsymbol{p} = 0$. Substitute $\boldsymbol{p} = 0$ into(53), and we have $\mu_v = 0$.

we have proven $\boldsymbol{p} = \mu_v = p_0 = 0$, which yields the contradiction to (52). Therefore, we get the conclusion that $[u_1^*(t)]^2 + [u_2^*(t)]^2 = u_3^*(t)$ holds almost everywhere on $[t_3, t_4]$.

In the same way, we can get the same conclusion through similar derivation when the performance index is $\int_{t_0}^{t_3} u_3 \mathrm{d}t, t \in [t_0, t_3]$. In sum, we get the conclusion that $[u_1^*(t)]^2 + [u_2^*(t)]^2 = u_3^*(t)$ holds almost everywhere on $[t_0, t_4]$, as claimed.

REFERENCES

[1] Y. Xiaodong and L. Shi, "A novel integral sliding mode-type continuous guidance law with autopilot lag for intercepting non-cooperative maneuvering targets," *IEEE Access*, vol. 7, pp. 126571–126581, 2019.
[2] Q. Zhao, X. Dong, Z. Liang, C. Bai, J. Chen, and Z. Ren, "Distributed cooperative guidance for multiple missiles with fixed and switching communication topologies," *Chin. J. Aeronautics*, vol. 30, no. 4, pp. 1570–1581, Aug. 2017.
[3] Q. Pan, D. Zhou, Y. Tang, and X. Li, "A novel antagonistic weapon-target assignment model considering uncertainty and its solution using decomposition co-evolution algorithm," *IEEE Access*, vol. 7, pp. 37498–37517, 2019.
[4] C. Z. Wei, J. F. Guo, and N. G. Cui, "Research on the missile formation keeping optimal control for cooperative engagement," *J. Astronaut.*, vol. 31, pp. 1043–1050, Apr. 2010.
[5] Y. Liu, Z. Luo, Z. Liu, J. Shi, and G. Cheng, "Cooperative routing problem for ground vehicle and unmanned aerial vehicle: The application on intelligence, surveillance, and reconnaissance missions," *IEEE Access*, vol. 7, pp. 63504–63518, 2019.
[6] Z. Zhao, J. Yang, Y. Niu, Y. Zhang, and L. Shen, "A hierarchical cooperative mission planning mechanism for multiple unmanned aerial vehicles," *Electronics*, vol. 8, no. 4, p. 443, Apr. 2019.
[7] B. Zhang, Q. Zong, L. Dou, B. Tian, D. Wang, and X. Zhao, "Trajectory optimization and finite-time control for unmanned helicopters formation," *IEEE Access*, vol. 7, pp. 93023–93034, 2019.
[8] J. Liu, W. Wang, X. Li, T. Wang, S. Bai, and Y. Wang, "Solving a multi-objective mission planning problem for UAV swarms with an improved NSGA-III algorithm," *Int. J. Comput. Intell. Syst.*, vol. 11, no. 1, p. 1067, May 2018.
[9] H. Yang, X. Bai, and H. Baoyin, "Rapid generation of time-optimal trajectories for asteroid landing via convex optimization," *J. Guid., Control, Dyn.*, vol. 40, no. 3, pp. 628–641, Mar. 2017.
[10] J. M. Carson, B. Acikmese, and L. Blackmore, "Lossless convexification of powered-descent guidance with non-convex thrust bound and pointing constraints," in *Proc. Amer. Control Conf.*, Jun. 2011, pp. 2651–2656.
[11] B. Acikmese, J. M. Carson, and L. Blackmore, "Lossless convexification of nonconvex control bound and pointing constraints of the soft landing optimal control problem," *IEEE Trans. Control Syst. Technol.*, vol. 21, no. 6, pp. 2104–2113, Nov. 2013.
[12] P. Lu and X. Liu, "Autonomous trajectory planning for rendezvous and proximity operations by conic optimization," *J. Guid., Control, Dyn.*, vol. 36, no. 2, pp. 375–389, Mar. 2013.
[13] M. Tillerson, G. Inalhan, and J. P. How, "Co-ordination and control of distributed spacecraft systems using convex optimization techniques," *Int. J. Robust Nonlinear Control*, vol. 12, nos. 2–3, pp. 207–242, Feb. 2002.
[14] D. Morgan, S.-J. Chung, and F. Y. Hadaegh, "Model predictive control of swarms of spacecraft using sequential convex programming," *J. Guid., Control, Dyn.*, vol. 37, no. 6, pp. 1725–1740, Nov. 2014.
[15] A. Ajorlou, K. Moezzi, A. G. Aghdam, and S. G. Nersesov, "Two-stage time-optimal formation reconfiguration strategy under acceleration and velocity constraints," in *Proc. 49th IEEE Conf. Decis. Control (CDC)*, Dec. 2010, pp. 7455–7460.
[16] D.-J. Zhao and Z.-Y. Song, "Reentry trajectory optimization with waypoint and no-fly zone constraints using multiphase convex programming," *Acta Astronautica*, vol. 137, pp. 60–69, Aug. 2017.
[17] D. Morgan, S.-J. Chung, and F. Hadaegh, "Spacecraft swarm guidance using a sequence of decentralized convex optimizations," in *Proc. AIAA/AAS Astrodyn. Spec. Conf.*, Aug. 2012, p. 4583.
[18] D. Morgan, G. P. Subramanian, S.-J. Chung, and F. Y. Hadaegh, "Swarm assignment and trajectory optimization using variable-swarm, distributed auction assignment and sequential convex programming," *Int. J. Robot. Res.*, vol. 35, no. 10, pp. 1261–1285, Sep. 2016.
[19] F. Augugliaro, A. P. Schoellig, and R. D'Andrea, "Generation of collision-free trajectories for a quadrocopter fleet: A sequential convex programming approach," in *Proc. IEEE/RSJ Int. Conf. Intell. Robots Syst.*, Oct. 2012, pp. 1917–1922.

[20] Y. Chen, M. Cutler, and J. P. How, "Decoupled multiagent path planning via incremental sequential convex programming," in *Proc. IEEE Int. Conf. Robot. Autom. (ICRA)*, May 2015, pp. 5954–5961.
[21] X. Wang, Y. Zhang, and H. Wu, "Distributed cooperative guidance of multiple anti-ship missiles with arbitrary impact angle constraint," *Aerosp. Sci. Technol.*, vol. 46, pp. 299–311, Oct. 2015.
[22] D. Guo, Z. Liang, P. Jiang, X. Dong, Q. Li, and Z. Ren, "Weapon-target assignment for multi-to-multi interception with grouping constraint," *IEEE Access*, vol. 7, pp. 34838–34849, 2019.
[23] Z. Wang, L. Liu, and T. Long, "Minimum-time trajectory planning for multi-unmanned-aerial-vehicle cooperation using sequential convex programming," *J. Guid., Control, Dyn.*, vol. 40, no. 11, pp. 2976–2982, Nov. 2017.
[24] R. Chai, A. Savvaris, and A. Tsourdos, "Solving multiobjective constrained trajectory optimization problem by an extended evolutionary algorithm," *IEEE Trans. Cybern.*, to be published.
[25] R. Chai, A. Savvaris, and A. Tsourdos, "Stochastic spacecraft trajectory optimization with the consideration of chance constraints," *IEEE Trans. Control Syst. Technol.*, to be published.
[26] T. R. Jorris and R. G. Cobb, "Three-dimensional trajectory optimization satisfying waypoint and no-fly zone constraints," *J. Guid., Control, Dyn.*, vol. 32, no. 2, pp. 551–572, Mar. 2009.
[27] R. Chai, A. Savvaris, A. Tsourdos, S. Chai, and Y. Xia, "Trajectory optimization of space maneuver vehicle using a hybrid optimal control solver," *IEEE Trans. Cybern.*, vol. 49, no. 2, pp. 467–480, Feb. 2019.

CHAOYUE LIU received the bachelor's degree from the Chang'an University of China, in 2014. He is currently pursuing the Ph.D. degree with the School of Aerospace Engineering, Beijing Institute of Technology. His main research interest includes in trajectory optimization and flight control.

CHENG ZHANG received the Ph.D. degree from the Beijing Institute of Technology of China, in 2005. He is currently a Professor with the School of Aerospace Engineering, Beijing Institute of Technology. His main research interests include flight dynamics and control, and overall design of flight vehicle.

FENFEN XIONG received the Ph.D. degree from the Beijing Institute of Technology of China, in 2010. She is currently an Associate Professor with the School of Aerospace Engineering, Beijing Institute of Technology. Her main research interests include robust trajectory optimization and uncertainty quantification.